Modeling the interinfluence of fertilizer-induced NH$_3$ emission, nitrogen deposition, and aerosol radiative effects using modified CESM2

Ka Ming Fung[1,a], Maria Val Martin[2], Amos P. K. Tai[1,3]

[1] Graduate Division of Earth and Atmospheric Sciences, The Chinese University of Hong Kong, Sha Tin, Hong Kong

[2] Leverhulme Centre for Climate Change Mitigation, School of Biosciences, University of Sheffield, Sheffield, UK

[3] Institute of Environment, Energy and Sustainability, and State Key Laboratory of Agrobiotechnology, The Chinese University of Hong Kong, Sha Tin, Hong Kong

[a] Now at: Department of Civil and Environmental Engineering, Massachusetts Institute of Technology, Cambridge, MA, USA

Correspondence to: Ka Ming Fung (kamingfung@link.cuhk.edu.hk), Maria Val Martin (m.valmartin@sheffield.ac.uk) & Amos P. K. Tai (amostai@cuhk.edu.hk)

Abstract. Global ammonia (NH$_3$) emission is expected to continue to rise due to intensified fertilization for growing food to satisfy the increasing demand worldwide. Previous studies focused mainly on estimating the land-to-atmosphere NH$_3$ injection but seldom addressed the other side of the bidirectional nitrogen exchange – deposition. Ignoring this significant input source of soil mineral nitrogen may lead to an underestimation of NH$_3$ emissions from natural sources. Here, we used an Earth system model to quantify NH$_3$-induced changes in atmospheric composition and the consequent impacts on the Earth's radiative budget and biosphere, as well as the impacts of deposition on NH$_3$ emissions from the land surface. We implemented a new scheme into the Community Land Model version 5 (CLM5) of the Community Earth System Model version 2 (CESM2) to estimate the volatilization of ammonium salt (NH$_4^+$) associated with synthetic and manure fertilizers into gaseous NH$_3$. We further parameterized the amount of emitted NH$_3$ captured in the plant canopy to derive a more accurate quantity of NH$_3$ that escapes to the atmosphere. Our modified CLM5 estimated that 14 Tg-N yr^{-1} of global NH$_3$ emission is attributable to fertilizers. Interactively coupling terrestrial NH$_3$ emissions to atmospheric chemistry simulations by the Community Atmospheric Model version 4 with chemistry (CAM4-chem), we found that such emissions favor the formation and deposition of NH$_4^+$ aerosol, which in turn influences the aerosol radiative effect and enhances soil NH$_3$ volatilization in regions downwind of fertilized croplands. Our fully coupled simulations showed that global-total NH$_3$ emission is enhanced by 3.3 Tg-N yr^{-1}, when 30% more synthetic

35   fertilizer is used compared to the 2000-level fertilization. In synergy with observations and emission inventories, our work provides a useful tool for stakeholders to evaluate the intertwined relations between agricultural trends, fertilize use, NH_3 emission, atmospheric aerosols, and climate, so as to derive optimal strategies for securing both food production and environmental sustainability.

1. Introduction

Global NH_3 emission has risen from 59 to 65 Tg-N yr^{-1} during 2000–2008, driven mainly by the increasing fertilizer use and manure handling in farms and animal operations (Sutton et al., 2013). After entering the atmosphere, NH_3 gas readily neutralizes sulfuric acid (H_2SO_4) and

45   nitric acid (HNO_3), which are derived from the oxidation of sulfur dioxide (SO_2) and nitrogen oxides (NO_x), forming inorganic sulfate-nitrate-ammonium (SNA) aerosols (Behera and Sharma, 2012). These secondary ammonium (NH_4^+) aerosols can constitute 25–75% of inorganic fine particulate matter ($PM_{2.5}$, particles with an aerodynamic diameter <2.5 µm) (Ianniello et al., 2011; Snider et al., 2016), which causes not only haze and smog that lower

50   visibility, but also respiratory and cardiovascular diseases that harm human health (Tie and Cao, 2009; Xing et al., 2016; Yang et al., 2019). In 2010 alone, an estimated 2.6 million premature deaths were associated with $PM_{2.5}$ pollution (Wang et al., 2017). Without proper controls, unbridled use of fertilizer to boost food production for the fast-growing population can further enhance global agricultural NH_3 emissions by ~12% in 2050 compared to year-

55   2010 level, posing an even greater health risk via $PM_{2.5}$ formation (Bodirsky et al., 2014). The global public health system may have to spend 20–290 billion USD more each year to compensate for the NH_3-derived detrimental effects on air quality and health (Gu et al., 2012; Paulot and Jacob, 2014; Guthrie et al., 2018).

Excessive atmospheric NH_3 also threatens ecosystems. The highly soluble NH_3 gas and

60   aerosol NH_4^+ (together known as NH_y) eventually return to the Earth's surface via dry and wet deposition, thus modifying the terrestrial nitrogen cycle. NH_y deposited on canopy foliage can be taken up and become readily available to promote photosynthesis (Wortman et al., 2012), but if highly concentrated it can also injure plant tissues and suppress biomass growth (Fangmeier et al., 1994; Krupa, 2003). Though NH_y deposition can enrich soil nutrients, it also

65   brings several adverse effects, including soil acidification and forest biodiversity loss (Tian and

Niu, 2015; Lu et al., 2008). Nitrifying bacteria often oxidize soil NH_4^+ in excess, and the

resulting NO_3^-, which is prone to leaching, can lower soil nutrient content as well as

contaminate groundwater, streams, rivers, and coastal waters, causing eutrophication (Lin et

al., 2001; Beeckman et al., 2018). NH_y directly falling onto natural waters is potentially toxic

70   to aquatic life even in low concentrations, and can deteriorate marine biodiversity (Zhang and

Liu, 1994; Shou et al., 2018).

The severity of the aforementioned consequences of excessive reactive nitrogen in the

environment has called for better management of these compounds, including better

monitoring and mitigation of agricultural NH_3. In the recent decade, the space-based Infrared

75   Atmospheric Sounding Interferometer (IASI) has been deployed to gauge atmospheric NH_3

concentration within air columns (Clarisse et al., 2009). This new ensemble of satellite

observations offers significant progress to address previous observational deficiencies and

allows daily monitoring of global NH_3 distribution (Clarisse et al., 2010; Van Damme et al.,

2014). Continued refinement in retrieval schemes and incorporation of machine-learning

80   techniques have further improved the sensitivity and reliability of measured NH_3

concentrations (Van Damme et al., 2017). It enables the creation of high-resolution maps of

atmospheric NH_3 and the possibility of pinpointing industrial and agricultural emission

hotspots with diameters smaller than 50 km (Van Damme et al., 2018). Their works have

provided valuable datasets not only for monitoring agricultural emissions but also for

85   benchmarking and improving emission inventories and numerical models.

NH_3 emission inventories are generally compiled by surveyed activity data and

empirical emission factors associated with primary sources including animal populations,

synthetic nitrogen fertilizers, biomass burning, and natural sources. A 1°-by-1° inventory,

which was among the first back then, estimated a global emission of 54 Tg-N yr^{-1} for 1990, of

90   which 34 Tg-N yr^{-1} is agricultural, excluding field burning, and 2.4 Tg-N yr^{-1} from natural soil

(Bouwman et al., 1997). Since then, much effort has been put into refining the estimation of

anthropogenic emissions. Recent inventories adjusted the estimated agricultural emissions

(including manure management, and both synthetic and manure fertilizers) in 2000–2010 to

33–37 Tg-N yr^{-1} (Sutton et al., 2013; Janssens-Maenhout et al., 2015; Hoesly et al., 2018). One

95   of the state-of-the-art inventories, the Emissions Database for Global Atmospheric Research

(EDGAR) version 4.3.2, provides global anthropogenic emission estimates in 0.1º-by-0.1º resolution for the period 1970–2012 (Crippa et al., 2018). The accuracy of these inventories is not only affected by the integrity of the activity data surveyed, but also constrained by the suitability of emission factors. Simply adopting emission factors from other countries may result in biases because of regional differences in technologies, farming practices, climate, and soil conditions (Huang et al., 2012). This pitfall has motivated the development of other national and regional inventories in the US (e.g., US Environmental Protection Agency (2014)), China (e.g., Zhang et al. (2018)), and Europe (e.g., European Environment Agency (2013)). These emission inventories are useful tools for source apportionment and input data for forward models but as the NH_3 emissions are prescribed they do not respond to changes in, e.g., nitrogen deposition and meteorology, making them insufficient for models to represent the full dynamics of the NH_y cycle.

The global NH_y cycle has proven to be challenging to study because of the various feedback mechanisms within the Earth system. The reactive nature of NH_3 and the contribution of deposited NH_4^+ to the re-emission of NH_3 from natural and agricultural soils have created a convoluted relationship between emissions and deposition. NH_4^+ particles can be transported along with airflows and dispersed across a more extensive geographical range than the highly reactive gaseous NH_3. Such transport can introduce large heterogeneity in the spatial distribution of reactive nitrogen, rendering it not only a local but pan-regional problem (Willem Asman; Mark A. Sutton, 1998). Moreover, NH_3 volatilization is a temperature-dependent process while the presence of atmospheric NH_3 affects the composition of aerosols and their radiative forcing, thus in turn modifying the Earth's surface energy budget (Ansari and Pandis, 1998).

In this study, we hence aim to enable modeling of the land-atmosphere bidirectional exchange of NH_y, so that we can quantify the dynamically evolving NH_y cycle and feedback mechanisms associated with it under a changing environment. We employed the Community Earth System Model version 2 (CESM2), which has state-of-the-art model components representing the land, atmosphere, sea ice, and oceans. These sub-models can run independently or in various coupled configurations (Hurrell et al., 2013). Many studies have employed CESM for studying processes in both the atmospheric and terrestrial nitrogen cycles, e.g., NO_x and N_2O emission (Saikawa et al., 2013, 2014; Zhao et al., 2017), deposition

(Lamarque et al., 2013), denitrification and nitrate leaching (Nevison et al., 2016), crop nitrogen uptake (Levis et al., 2018), and reactive nitrogen input to ecosystem associated with synthetic and manure fertilizers (Riddick et al., 2016; Vira et al., 2020, 2021). Yet, these studies did not consider the dynamic bidirectional transfer of NH_3 and NH_4^+ between the land and atmosphere. To add the dynamic cycle of NH_y back to CESM2, we adopted a process-based approach to parameterize NH_3 emission from cropland soils, which is different from the bidirectional "voltage-resistance" models (Zhu et al., 2015; Riddick et al., 2016; Pleim et al., 2019; Vira et al., 2020). Our approach determines the multi-stage processes of soil NH_4^+ to NH_3, including adsorption, dissociation, and volatilization. The process-based nature of this scheme allows us to evaluate the response of NH_3 emission to soil climate, soil nitrogen content, fertilization, deposition, competition against other soil biogeochemical processes (nitrification, microbial uptake, etc.), and vegetation growth. Comparing to other approaches, our scheme, which borrowed from a biogeochemical model, the DeNitrification-DeComposition (DNDC), requires variables that are mostly already modeled in CLM5, allowing us to largely capture the dynamic nature of NH_3 emission. We also developed a prognostic parameterization for canopy capture of NH_3, instead of using a fixed generic value (e.g., one constant canopy reduction factor for all plants as used in some other studies (e.g., Riddick et al., 2016; Bouwman et al., 1997). Implementing these new schemes in the Community Land Model version (CLM5) (Lawrence et al., 2019), we could then estimate the emission associated with fertilizer use and perform fully coupled simulations with the Community Atmosphere Model version 4 with Chemistry (CAM4-chem) (Lamarque et al., 2012) that allow two-way exchange of NH_y bridged by online emission and deposition to understand the subsequent effects on aerosol formation, climate, terrestrial ecosystems, and crop growth. We also compared our results with available emission inventories to evaluate model accuracy and uncertainty.

This paper demonstrates a framework that could help unfold the complicated interactions between fertilizer use, NH_3 emission, aerosol formation, climate, terrestrial ecosystems, and crop production. For instance, a recent study based on our model framework showed that enhanced nitrogen deposition induced by future fertilize use could modify the meteorological environment, via changes in vegetation and soil biogeochemistry, and modulate future ozone pollution (Liu et al., 2021).

2. Methods

2.1 Community Earth System Model

160   We introduced new functionalities into CESM2 to enable the simulation of a coupled land-atmosphere nitrogen cycle, and to further investigate the impacts of fertilizer-induced NH_3 emission on atmospheric composition, terrestrial biogeochemistry, and climate change. In particular, we implemented into CLM5 new parameterization schemes to quantify NH_3 volatilized from soil due to fertilizer application and captured by plant canopies. We further

165   bridged CLM5 and CAM4-chem to enable two-way exchange of soil NH_3 emission and deposition of NH_4^+ to model a fully coupled, prognostic land-atmospheric NH_y cycle.

Our model development was based on CLM5 with active biogeochemical cycles and crop sub-model (CLM5-BGC-Crop or CLM5 in short), which represents terrestrial carbon and nitrogen cycling with prognostic vegetation and crop growth. The model uses a sub-grid

170   hierarchy (from grid cells, land units, columns, to patches) to capture the biogeophysical and biogeochemical differences between various land types within a model grid cell. In particular, CLM5 handles natural soil and croplands differently: multiple natural vegetation patches are configured to occupy a single unmanaged soil column sharing a single pool of nutrients while each crop patch has a dedicated column. Such setting allows no resource competition between

175   natural vegetation and crops, nor among crops (Drewniak et al., 2013). There are 16 types of natural vegetation (including bare ground) and eight active crops (temperate soybean, tropical soybean, temperate corn, tropical corn, spring wheat, cotton, rice, and sugarcane) in this model (Lombardozzi et al., 2020). Vegetation and crops are represented by plant functional types (PFTs), each having specific ecophysiological, phenological and biogeochemical parameters

180   (Levis et al., 2018). Default PFT distribution of natural vegetation and crops are derived from satellite observations (e.g., MODIS) and agricultural census data (Lawrence and Chase, 2007; Portmann et al., 2010). The beginning of plant growth stages (seedling, leaf emerging, and grain filling), as well as crop sowing dates and planting durations, are controlled by cumulative warm-enough hours at the beginning of spring. Crops obtain nutrients from the soil mineral

185   nitrogen pool, which is supplied by nitrogen deposition and fertilization. Fertilizer is applied to each patch for 20 consecutive days evenly when the crops enter the leaf emergence phase. Synthetic fertilizer input was prescribed by crop type and country at the 2000-level based on Land-Use Harmonization (LUH2) fertilization rates (Hurtt et al., 2011). Manure fertilizer

application rate is assumed constant for all crops at 2 g-N m^{-2} yr^{-1}, same as the model default (Lombardozzi et al., 2020). All added depositional and fertilizers N are added to the soil NH_4^+ pool of each layer from ground surface to 0.4 m underground according to a model-defined soil profile (**Table S1**) (Lawrence et al., 2018). Crops are harvested once they reach maturity or predefined maximum growing days (typically 150–165 days) (Lawrence et al., 2018).

In addition to the NH_3 schemes, we also modified CLM5 to better simulate the terrestrial nitrogen cycle, specifically on the emission of NO_x from denitrification and nitrification and microbial mineralization of soil nitrogen. These modifications are documented in **Supplementary Information**.

2.2 Soil ammonia emission and canopy capture

Figure 1 summarizes the primary pathways of the terrestrial nitrogen cycle in CLM5. The model tracks nitrogen content in soil, plant, and organic matter as an array of separate nitrogen pools, and biogeochemical processes as exchange fluxes of nitrogen between these pools. Soil mineral nitrogen, NH_4^+, and NO_3^- are competed for among plant uptake, microbial immobilization, nitrification, and denitrification, based on the relative demand from each process. Release of nitrous oxide (N_2O) and NO_x as byproducts of nitrification and denitrification and leaching of soil nitrate also deplete soil NH_4^+ and NO_3^-, which can be replenished by fertilization and deposition of atmospheric NH_y and NO_x. The deposition rates were prescribed in the default configuration and dynamically computed by CAM4-chem in our version. Other sources of soil mineral nitrogen include biological fixation by microbes or soybean and decomposition of plant litter and soil organic matter. Our proposed NH_3 emission scheme was borrowed from a standalone biogeochemical model, DNDC version 9.5 (Li et al., 2012; Gilhespy et al., 2014; source code of DNDC v9.5 provided by Changsheng Li via personal communication on Jun 18th, 2015), which has been extensively used for studying agricultural NH_3 emission (e.g., Li et al., 2012; Balasubramanian et al., 2015; Zhang and Niu, 2016; Balasubramanian et al., 2017).
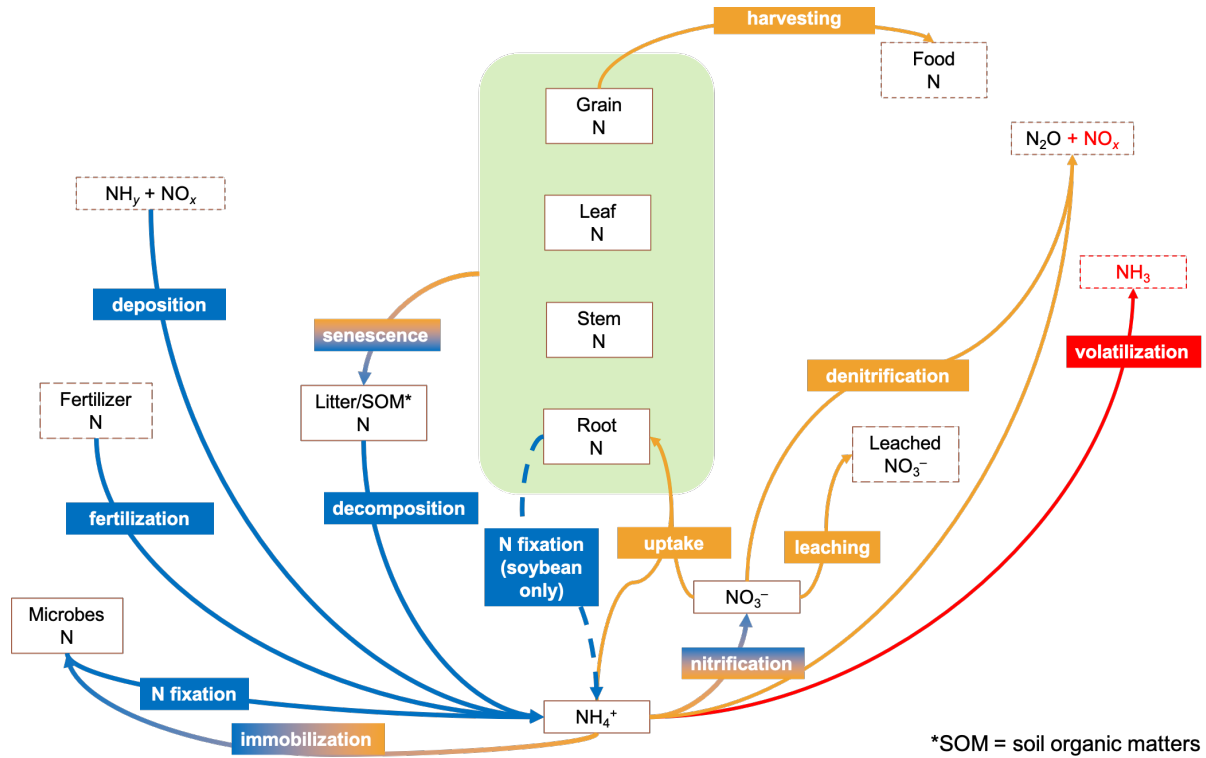
Figure 1. Major pathways modeled by CLM5 nitrogen (N) cycle. Blue arrows indicate N entering the soil N nitrogen pool while orange arrows are for leaving. The default model tracks only N pools in boxes enclosed by solid lines, but not those with dashed lines. N contents in crop tissues are modeled as pools inside the green regions. The red arrow indicates the missing pathway of NH_3 volatilization in the default model. Nitrogen gas (N_2) emitted by denitrification is not shown. SOM denotes soil organic matters.

Following the treatment in DNDC, our scheme considered NH_3 volatilization a multistage process, and estimated the potential soil NH_3 prone to emission ($F_{soil,pot}$; g-N m^{-3}) based on soil NH_4^+ content. In each soil layer of a column or patch:

$$F_{soil,pot} = \left[NH_{4\,(soil)}^+\right](1 - f_{ads})f_{dis}f_{vol} \tag{1}$$

where $[NH_{4\,(soil)}^+]$ (g-N m^{-3}) is the amount of soil NH_4^+; f_{ads} accounts for the portion of NH_4^+ adsorbed onto the surface of soil matrix; f_{dis} is the fraction of the non-adsorbed NH_4^+ that dissociated into aqueous NH_3, and; f_{vol} is the fraction of aqueous NH_3 volatilized as gaseous NH_3. The adsorbed fraction f_{ads}, which is also bounded between 0 and 1, is given by Li et al., 1992 and Dutta et al., (2016):

$$f_{ads} = 0.99(7.2733f_{clay}^3 - 11.22f_{clay}^2 + 5.7198f_{clay} + 0.0263) \tag{2}$$

where f_{clay} is soil clay fraction as prescribed by the CLM surface data (Bonan et al., 2002); we adopted a factor of 0.99 instead of the one reported in Dutta et al. (2016), as per the source code of DNDC.

The non-adsorbed NH_4^+ dissociates reversibly into aqueous NH_3 and hydrogen ion ($NH_4^+{}_{(aq)} \rightleftharpoons NH_{3(aq)} + H^+$), and hence, f_{dis} is determined by the following equations (Li et al., 2012; Sutton, 1990; Sutton et al., 1993):

$$f_{dis} = \frac{K_w}{K_a[H^+]} \tag{3}$$

$$K_w = 10^{0.08946+0.03605[°C^{-1}]T_{soil}} \times 10^{-15} \tag{4}$$

$$K_a = (1.416 + 0.01357[°C^{-1}]T_{soil}) \times 10^{-5} \tag{5}$$

$$[H^+] = 10^{-pH} \tag{6}$$

where K_a (mol L^{-1}) and K_w (mol L^{-2}) are dissociation constants for NH_4^+/NH_3 and hydrogen-/hydroxide-ion equilibria, respectively; T_{soil} (°C) is soil temperature; $[H^+]$ (mol) is the concentration of aqueous hydrogen ion in the soil calculated from soil pH. CLM5 is currently not capable of calculating soil pH implicitly so we performed our simulations using a constant pH of 6.5 for a more focused analysis. This pH value is consistent with the value used in the nitrification and denitrification schemes in CLM5. We further evaluated the uncertainty induced by our choice of pH and presented the sensitivity test results in **Supplementary Information**. Briefly, a higher pH would promote model NH_3 emission rate exponentially as the emission rate is of the order of 10^{pH}. This high sensitivity warrants the need to include crucial chemical processes in the model for accurately determining soil pH online.

Lastly, we used this equation to calculate f_{vol} (Li et al., 1992; Gardner, 1965; source code of DNDC v9.5):

$$f_{vol} = \left(\frac{1.5s}{1\,[m\,s^{-1}]+s}\right)\left(\frac{T_{soil}}{50\,[°C]+T_{soil}}\right)\left(\frac{l_{max}-l}{l_{max}}\right) \tag{7}$$

where s (m s^{-1}) is surface wind speed; T_{soil} (°C) is soil temperature; l and l_{max} (both in m) are the depth of each soil layer and the maximum depth of a soil column, respectively. Our scheme assumes that vaporized soil NH_3 in a deeper layer diffuse upward to the surface, but does not

explicitly simulates the process. Instead, it is represented in the last term in **Eq. (7)** as a ratio of $(l_{max} - l)/l$ for the $NH_{3(g)}$ contained in each soil layer. Hence, soil NH_4^+ in deeper layers is also subject to loss to NH_3 volatilization but at much slower rates than that in the upper layers. Details of the soil profile are provided in **Table S1**.

The actual soil NH_3 to be emitted ($F_{soil,act}$; g-N m^{-3}) from each soil layer is then determined as:

$$F_{soil,act} = \min(F_{soil,pot}, [NH_4^+]_{available}) \tag{8}$$

where $F_{soil,pot}$ is from **Eq. (1)** and $[NH_4^+]_{available}$ (g-N m^{-3}) is the concentration of available soil NH_4^+ in the soil layer. The model distributes available soil NH_4^+ to all competing processes, namely, NH_3 emission, plant uptake, microbial immobilization, and nitrification, according to their relative demands (individual potential flux to sum of all four potential fluxes) without bias toward any process (Lawrence et al., 2019). The column-level actual soil NH_3 prone to emission (F_{soil}; g-N m^{-2}) is then computed as the sum of the product of $F_{soil,act}$ and the soil layer thickness (in meters) across all vertical layers.

Finally, assuming such NH_3 is released to the atmosphere at a constant rate over a model time step size ($\Delta t = 1800$ s in this study), our model estimates the NH_3 emission flux ($\dot{F}_{soil}$; g-N m^{-2} s^{-1}) as:

$$\dot{F}_{soil} = \frac{F_{soil}}{\Delta t} \tag{9}$$

If vegetation is present above the soil, some of the emitted NH_3 can be retained by the plant canopy, which is known to be related to the adsorption of hydrophilic NH_3 onto the leaf surface and molecular diffusion via the leaf stomata (Van Hove et al., 1987). Some studies represented the amount of captured NH_3 using constant scaling factors (e.g., 0.6 for all vegetation in Riddick et al. (2016), 0.8, 0.5, and 0.2 for tropical rainforests, other forests, and all other vegetation types, respectively, in Bouwman et al. (1997)). Here, we calculated the flux of NH_3 captured by canopy following the equation used in DNDC that accounts for the change in in-canopy NH_3 concentration, deposition velocity of ammonia, leaf area index (LAI), and air moisture (Institute for the Study of Earth, Oceans, and Space, University of New Hampshire, 2017). To include the dynamic growth of crop canopy, we further adopted the canopy height

adjustment factor employed by the Community Multiscale Air Quality (CMAQ) regional chemical transport model (Pleim et al., 2013). The portion of NH_3 flux from the soil that is not captured by plant canopies ($\dot{F}_{atm}$; g-N m^{-2} s^{-1}) is thus:

290
$$\dot{F}_{atm} = \dot{F}_{soil}(1 - f_{can}) \tag{10}$$

$$f_{can} = \frac{L}{s_{10}} v_c \varphi_c b (h_{top} - h_{bot}) \tag{11}$$

where L is one-sided snow-free LAI, s_{10} is the wind-speed (m s^{-1}) at 10-m height, v_c is the deposition velocity of NH_3 (0.05 m s^{-1} as in DNDC), φ_c is in-canopy relative humidity, b is a correction factor for the effect of canopy thickness (14 m^{-1} is used here as suggested by Pleim

295   et al. (2013)), and h_{top} and h_{bot} are heights of canopy top and bottom (both in m), respectively. Except for v_c and b, all variables are calculated within CLM5 (see Lawrence et al. (2019) for detailed calculation methods). These two equations estimate the concentration of NH_3 exposed to plant canopy under a given soil emission rate at each time step: dividing soil NH_3 emission rate by s_{10} gives an approximate in-canopy NH_3 concentration, and multiplying the latter with

300   v_c and L produces an estimated quantity of NH_3 retained by the canopy. The last three terms account for the influence of in-canopy moisture and canopy thickness on the effectiveness of canopy capturing. We used $\dot{F}_{atm}$ as an input of the ammonia emissions to drive chemistry calculations in CAM4-chem. The captured NH_3 can re-enter the soil surface along with water throughfall or be metabolized by the plants if it diffuses into the leaf tissues (Hutchinson et al.,

305   1972). Since the detailed mechanisms are still uncertain and beyond the focus of this study, we decided to assume that all captured NH_3 returns to the soil directly as NH_4^+ and will discuss how it will affect our analysis in **Conclusions**.

2.3 Simulations of the land-atmosphere NH_y cycle

310   For the atmospheric component, we employed CAM4-chem (Lamarque et al., 2012), with chemistry based on the tropospheric chemistry mechanism of MOZART-4 (Emmons et al., 2010). CAM4-chem employs a bulk aerosol approach and predicts the formation of $PM_{2.5}$ components including SO_4^{2-}, NO_3^-, and NH_4^+, where the injection rates of precursors – sulfur dioxide (SO_2), NO_x, and NH_3 – are prescribed by the Coupled Model Intercomparison Project

phase 6 (CMIP6)/Community Emissions Data System (CEDS) emission inventory (CMIP6 hereinafter) for anthropogenic activities (Hoesly et al., 2018). The biomass burning emissions used for our simulations are described by von Marle et al. (2016, 2017) and are all assumed as surface emissions without plume-rise nor predefined vertical distribution. Biogenic emissions, e.g., of isoprene, are updated online from CLM5 using the Model of Emissions of Gases and Aerosols from Nature (MEGAN) version 2.1 (Guenther et al., 2012). In our coupled simulations, we substituted the portion of NH_3 emission associated with fertilizers from the CAM4-chem inventory input (CESD) for our online simulated emission rates from CLM5. This study did not consider manure spreading on pastures and grazing animals. Atmospheric NH_3 and NH_4^+ formed sequentially return to CLM5 through deposition. We note that the NO_x emission inputs for CAM4-chem were solely from the emission inventories and did not include those from our modified denitrification and nitrification schemes.

Dry deposition in CAM4-chem is handled using the resistance approach (Wesely, 1989; Emmons et al., 2010). For NH_3 vapor, the model calculates the aerodynamic and the boundary-layer (laminar sublayer) resistance based on the online atmospheric dynamics, while the surface resistance over land is determined according to the online CLM5 surface variables, e.g., canopy height and LAI, as well as species-specific reactivity factor for oxidation and effective Henry's Law coefficients. For particle-phase NH_4^+, the aerodynamic resistance is the same as that of NH_3, but the boundary-layer and surface resistances are replaced by a single resistance term that depends on the surface friction velocity. The deposition velocities of NH_3 and NH_4^+ are the reciprocal of the sum of their corresponding resistance terms, and their deposition rates are the product of their deposition velocities and concentrations. Wet deposition in CAM4-chem follows the Neu and Prather (2012) scheme, which assumes a first-order loss of chemicals due to in-cloud and below-cloud scavenging processes. The wet deposition rates of NH_3 and NH_4^+ are the products of their concentration, their loss frequencies (based on their Henry's Law coefficients), and the fraction of the grid box subject to scavenging (e.g., cloudy or raining). These NH_y deposition fluxes (together with NO_x) then become the input to CLM5 for the soil NH_4^+ pool (Lawrence et al., 2018).

In the default configuration, atmospheric chemistry interacts with the climate solely through radiation in CAM4-chem (Lamarque et al., 2012). Furthermore, atmospheric reactive nitrogen (NH_4^+ or NO_3^-) does not directly interact with radiative transfer in the model. Instead,

its radiative implications are manifested via altering the gas-aqueous partitioning of sulfate (Emmons et al., 2010; Metzger, 2002) and the subsequent changes in direct radiative effect due to any changes in sulfate aerosols. The subsequent sulfate-induced changes in cloud optical properties (indirect radiative effect) were not considered in this work. Detailed description of the radiative transfer processes in CAM4-chem is provided in Neale et al. (2010).

Recent studies on NH_3 emission using CESM2 (e.g., Riddick et al. (2016) and Vira et al. (2020)) focused only on the one-way land-to-atmosphere flux of NH_3 while neglecting the enhancing effect of nitrogen deposition on NH_3 emission. By coupling CLM5 and CAM4-chem, we allowed the model land-atmosphere NH_y cycle to evolve in response to any changes in the bidirectional exchange of NH_3 and NH_4^+ via online emission and deposition. It also makes our method more suitable than a one-way model for studying the feedback effects of future changes in climate and agricultural activities on the biogeochemical cycles.

Table 1 provides configuration details of our experiments. [CAM4_CLM5_2000] and [CAM4_CLM5_2050] encapsulated the full functionality of our implementation, i.e., CAM4-chem receives the online CLM5 NH_3 emission rates as input to predict atmospheric NH_3 concentration, the subsequent formation of secondary ammonium aerosols (modeled as changes in sulfate aerosols in the model), and the corresponding instantaneous sulfate aerosol radiative effect, whilst CLM5 obtains the online CAM4-chem dry and wet deposition rates of NH_y and NO_x to calculate the addition of soil NH_4^+ via deposition. The deposited nitrogen will eventually enrich soil fertility and fuel the re-emission of soil NH_3 while the aforementioned aerosol radiative effect can cool the Earth's surface and suppress NH_3 volatilization. The [CAM4_CLM5_NDEP] cases were set to isolate the impact of NH_y deposition on NH_3 emission and crop growth. In this setup, CAM4-chem used prescribed gases (except for water vapor) and aerosols in the radiation transfer calculation (i.e., aerosol-radiation interaction is disabled). Hence, any changes in the atmospheric sulfate aerosol loading induced by the addition/reduction of NH_3 would not affect radiative transfer. We note that the differences in radiative budget between the [CAM4_CLM5_NDEP] and other configurations with aerosol-radiation interaction enabled would include the effects attributable to both NH_3-induced sulfate changes as well as the differences in spatial distribution between the prescribed and prognostic aerosols. For instance, the differences between [CAM4_CLM5_NDEP] and [CAM4_CLM5] are substantial for sulfate (up to 4% in zonal mean mass ratio; mostly inland) and dust (up to

30% zonally; mostly in Sub-Saharan Africa and other desert regions), and are unlikely related to NH_3 changes; meanwhile, the differences are rather negligible for organic carbon, black carbon, and sea salt. This configuration was intended to isolate the enhanced fertilization effect of N deposition. Similarly, [CAM4_CLM5_CLIM] cases were prescribed with constant nitrogen deposition fluxes so that we could quantify the impacts of the changes in instantaneous aerosol radiative effects. We hypothesized that an increased NH_3 emission would promote the formation of sulfate aerosols, and the subsequent aerosol cooling effect would be observed in this setup. Finally, we further evaluated the impacts of intensive fertilizer use to promote agricultural production in the future as projected by FAO (2007) by repeating the first three simulations with fertilization at present-day (2000; model default) and future (2050; assuming 30% more synthetic fertilizers while manure fertilizer is kept at 2000-level) rates. We note that future increases in agricultural production might also involve cropland expansion, but such practice was not included in this study.

Table 1. Details of simulation designs.

Alias	Synthetic Fertilizer Usage	Fertilizer-induced NH_3 Emission	N-deposition	Aerosol-radiation Interaction
CAM4_CLM5_2000	Same as 2000-level	Modified CLM5 in this study	Dynamic	Enabled
CAM4_CLM5_2050	30% more than 2000-level	Modified CLM5 in this study	Dynamic	Enabled
CAM4_CLM5_NDEP_2000	Same as 2000-level	Modified CLM5 in this study	Dynamic	Disabled
CAM4_CLM5_NDEP_2050	30% more than 2000-level	Modified CLM5 in this study	Dynamic	Disabled
CAM4_CLM5_CLIM_2000	Same as 2000-level	Modified CLM5 in this study	From [CAM4_CLM5] assuming 2000-level fertilization	Enabled
CAM4_CLM5_CLIM_2050	30% more than 2000-level	Modified CLM5 in this study	From [CAM4_CLM5] assuming 2000-level fertilization	Enabled
CAM4_CMIP6_2000	Same as 2000-level	CMIP6 inventory	Dynamic	Enabled

All simulations were run for 30 years using the spun-up year-2000 initial conditions with the corresponding land cover data provided out-of-the-box by CLM5. The first 10 years

of outputs were used to further stabilize the model (such that the interannual variability of the emission fluxes could be $< \pm 10\%$) after our ammonia scheme was implemented. Our analysis in the next section focuses on the averages of the last 20 years of simulated results to minimize influence from any long-term meteorological variability. Only the atmosphere (CAM4-chem) and the land (CLM5) components were active. CAM4-chem was run with free dynamics in the standard spatial resolution of 1.9º by 2.5º horizontally with 27 vertical layers (from surface to ~40 km). CLM5 was run in the same horizontal resolution with 25 soil layers down to ~50 m below ground. Sea surface temperature (SST) and sea ice conditions (Hurrell et al., 2008), as well as the mixing ratios of greenhouse gases (Meinshausen et al., 2017) were all fixed at the 2000-levels. Our analysis focuses on the changes in fluxes of soil biogeochemical processes, the evolution of atmospheric NH_3, the sequential changes in sulfate aerosols, and the influence of the bidirectional NH_y exchange on crop production.

2.4 Datasets for model validation

We also compared our simulation results with various available global observations and emission inventories. CLM5-modeled NH_3 emission was compared with multiple emission inventories including CMIP6, EDGAR, and the Magnitude And Seasonality of Agricultural Emissions for NH_3 (MASAGE). CAM4-chem-simulated atmospheric NH_3 using CLM5 NH_3 and CMIP6 were compared against the satellite-derived IASI-NH_3 concentration field (gridded and reported in Van Damme et al. (2018)). Details of these datasets are tabulated in **Table 2**. The datasets were regridded to match our model resolution of 1.9º by 2.5º using bilinear interpolation. We note also that model-inventory comparisons are not meant to be exact given that our simulations were performed using free-running dynamics and thus did not necessarily match the meteorological years of the inventories, and the synthetic fertilizer use was not identical to the ones assumed when inventories were compiled. Thus, these results are presented as qualitative comparisons to indicate where our estimation is consistent with the inventories and where it is not.

Table 2. Details of observations and emission inventories used in this study for model comparison and validation.

Name	Coverage	Resolution	Period of data	Data type: sources extracted for model comparison
MASAGE (Paulot et al., 2014)	Global	0.5º-by-0.5º Monthly mean	2006	Emission inventory: NH_3 emission from agricultural soil associated with synthetic fertilizer only
EDGAR (Crippa et al., 2018)	Global	0.1º-by-0.1º Monthly mean	2010	Emission inventory: NH_3 emission from agricultural soil with both synthetic and manure fertilizers
CMIP6 (Hoesly et al., 2018)	Global	0.01º-by-0.01º Monthly mean	2000–2015	Emission inventory: NH_3 emission from agricultural soil with both synthetic and manure fertilizers
IASI (Van Damme et al., 2018)	Global	0.01º-by-0.01º Annual mean	2008–2016	Satellite-based measurement: Column NH_3 density

3. Results

3.1 Fertilizer-induced NH₃ emission

We first evaluated the fertilizer-induced NH_3 emission simulated by the fully coupled land-atmosphere simulation, [CAM4_CLM5_2000]. **Figure 2** shows the annual-total global NH_3 emission at above-canopy level from different land types averaged over the remaining 20 years of simulation. We also compared our NH_3 emission with inventory estimates reported by CMIP6 (Hoesly et al., 2018), EDGAR v4.3.2 (Crippa et al., 2018), and MASAGE (Paulot et al., 2014). We extracted the monthly fertilizer-induced NH_3 emission estimates from MASAGE, and assumed that one-third of the total agricultural NH_3 emission reported by CMIP6 and EDGAR are associated with synthetic fertilizer, which is consistent with the apportionment reported in previous studies and environmental reports (Paulot et al., 2014; Riddick et al., 2016; National Oceanic and Atmospheric Administration, 2000; European Environment Agency, 2010; Gu et al., 2012; Paulot et al., 2015; Zheng et al., 2017).

Regional emission totals are summarized in **Table 3**. A grid cell-by-grid cell model-inventory spatial comparison of the annual-total NH_3 emission rates was conducted by computing Pearson's correlation coefficients (R) and slopes (β) of linear regression using the reduced major axis method as well as normalized mean biases (NMB; $\Sigma(M_i - O_i)/\Sigma(O_i)$, where M_i and O_i are simulated and inventory NH_3 emission in each grid cell) and mean fractional biases (MFB; $2\Sigma[(M_i - O_i)/(M_i + O_i)]/N$, where N is the number of grid cell). A summary of

these statistics is shown in **Figure 2(a)**. We also computed the R values between the monthly emission rates computed by CLM5 (as in the fully coupled case, [CAM4_CLM5_2000]) and each inventory for each grid cell (see **Figure 2(d)**, **(f)**, and **(h)**). We highlighted with overlaying black dots the grid cells with high coefficients of determination, which are statistically significant (i.e., $R^2 > 0.5$ and $p < 0.05$), indicating where our simulation can reproduce more than half of the variability of the inventory estimates.

Table 3. Regional fertilizer-induced NH_3 emission totals (Tg-N yr^{-1}) estimated by our model and reported by other inventories.

	Global	USA	Europe	India	China
CAM4_CLM5_2000[a]	14.2 ($\pm$ 0.60)	2.1 ($\pm$ 0.35)	0.6 ($\pm$ 0.07)	2.8 ($\pm$ 0.28)	1.2 ($\pm$ 0.08)
CMIP6[b]	10.9 ($\pm$ 0.65)	0.9 ($\pm$ 0.05)	0.7 ($\pm$ 0.16)	1.9 ($\pm$ 0.15)	2.6 ($\pm$ 0.30)
EDGAR[c]	10.5	0.7	0.5	1.6	3.0
MASAGE	9.1	0.5	0.4	1.7	2.8

a   20-year 1-SD are shown in the brackets
b   16-year 1-SD are shown in the brackets (2000–2015)
c   Variation in 2012 of both cultural statistics and emission factors ranged from 186% to 294% (Crippa et al., 2018)

Globally, CLM5 estimates that the annual-total fertilizer-induced NH_3 emission reaches 14 Tg-N yr^{-1} while the global fertilizer input is 96 Tg-N yr^{-1} (of which 71% is synthetic fertilizers). Our estimation is close to the 12 Tg-N yr^{-1} (from synthetic fertilizer only) and 18 Tg-N yr^{-1} (11 Tg-N yr^{-1} from both synthetic fertilizer and 6.5 Tg-N yr^{-1} from manure application) reported by two similar studies, Riddick et al. (2016) and Vira et al. (2020), respectively. Our estimate is higher than all three inventories of NH_3 emissions associated with synthetic fertilizers, which are 10 Tg-N yr^{-1} for CMIP6 and EDGAR, and 9.1 Tg-N yr^{-1} for MASAGE. The global R values are positive and lie within 0.4–0.6 across all inventories, indicating a fairly good correlation between CLM5 and all three inventories, especially CMIP6 and MASAGE. Systematic model high-biases are implied by the greater-than-unity β values, with small NMB and MFB values ranging between +32~+56% and –22~+32%, respectively.

Top food-producing countries are responsible for a major portion of the fertilizer-induced NH_3 emission: 20 % of CLM5 global total was from India (2.8 Tg-N yr^{-1}), 15 % from the US (2.1 Tg-N yr^{-1}), and 8.6% from China (1.2 Tg-N yr^{-1}). Emission hotspots are found

close to their cropping regions in the model and the inventories, but their spatial gradients are different. In India, CLM5 shows more concentrated emission sources over the northern regions, resulting in higher local emission rates than the inventories. This distribution pattern resembles the India's north-higher south-lower fertilization gradient adopted by the model. In contrast, CMIP6 estimates a more evenly distributed emission spatial pattern over India, and higher emission rates over the southern regions. EDGAR and MASAGE show a spatial gradient of NH_3 emission decreasing from north to south. Such gradients may explain their low R and high β values against our revised CLM5. Despite the spatial mismatch, the NMB (+68~+74%) and MFB (+14~+15%) for the model estimation over India are relatively small.

CLM5 estimates more intense emission hotspots in the US, which are located near the "Corn Belt" of the central US and southern California. US emission rates by CLM5 are much higher than the other three inventories, as seen in the difference maps in **Figure 2**, as indicated by the large β (>3.2), and large regional NMB. Differences in the spatial distribution of NH_3 emission are also observed over China. CLM5 estimates that more NH_3 is emitted from central and northeastern China, while the emission hotspots in CMIP6 and EDGAR are found in northeastern China and those of MASAGE are in eastern China. Such deviation may be attributable to different fertilizer usage schedules used by CLM5 and other inventories. For example, MASAGE considers multiple-type fertilizers that can be more or less prone to NH_3 loss than urea (Bouwman et al., 2002), and assumes a three-stage fertilization at sowing, growth, and harvesting (Paulot et al., 2014). EDGAR also reported a high uncertainty (~97%) of present-day NH_3 emissions in China due to incomplete information about the agricultural sector (Crippa et al., 2018).
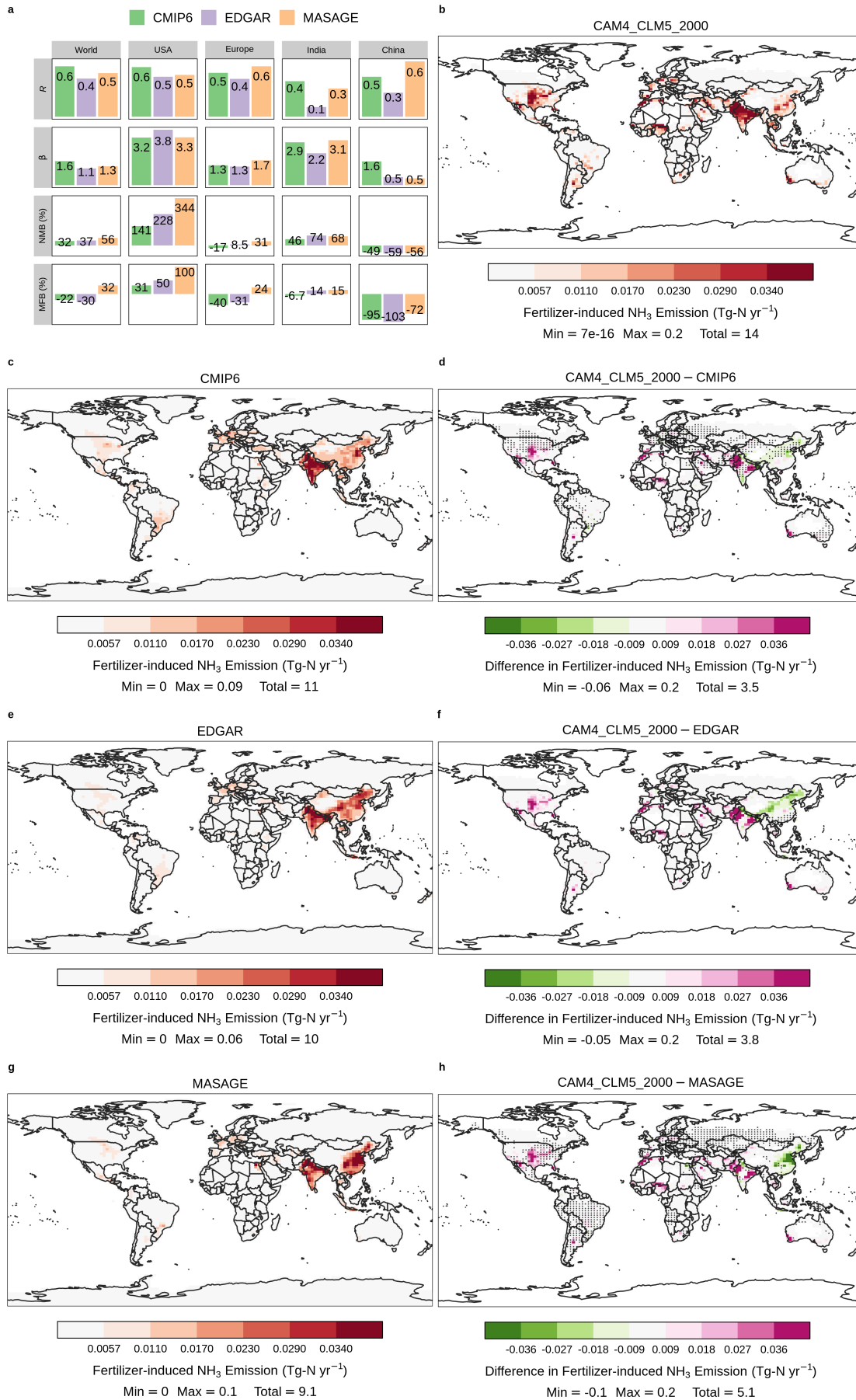
Figure 2. Fertilizer-induced NH_3 emission estimated by CLM5 (synthetic and manure) and other emission inventories (synthetic only). Correlation analysis between CLM5-simulated annual-total emission and other inventories with regional breakdowns is summarized in panel **(a)**. Spatial distribution of annual-total fertilizer-induced NH_3 emission simulated by [CAM4_CLM5_2000], and estimated by CMIP6, EDGAR, and MASAGE are illustrated in panels **(b)**, **(c)**, **(e)**, and **(g)**, respectively. Panels **(d)**, **(f)**, and **(h)** show the spatial distribution of differences in annual-total NH_3 between CLM5 and CMIP6, EDGAR, and MASAGE, correspondingly. Overlaying black dots in the difference maps indicate grid-cells with a high statistically significant spatiotemporal correlation (i.e., $R^2 > 50\%$, $p < 0.05$) between CLM5 and the corresponding inventories. Color scales are saturated at respective values, and ranges of values are shown in the legend titles.

Figure 3 shows the seasonality of NH_3 emission associated with artificial fertilizer in the Northern and Southern Hemisphere. CLM5 assumes each crop receives a specific amount of fertilizer (as soil NH_4^+) applied evenly for 20 consecutive days since leaf emergence. This soil NH_4^+ input speeds up plant uptake, microbial immobilization, nitrification, as well as NH_3 volatilization, explaining the Northern Hemisphere peaking in emission in April and May and Southern Hemisphere peaking in October, overlapping with the regional cropping seasons. All inventories show springtime peaks in each hemisphere, but the peak of EDGAR always leads the others by a month. CMIP6 has multiple peaks (two in the Northern Hemisphere and three in the Southern Hemisphere). These deviations exist mainly because of the differences in planting schedule and duration of fertilization used by the inventories. The higher CLM5 peaks are consistent with the systematic overestimation discussed above. NH_3 emission returns to "background" levels when it is not in the planting seasons. EDGAR and CMIP6 have higher background levels than MASAGE because the original estimates used in this study accounted for not only synthetic fertilizer but also manure application (for both) and management (for CMIP6 only), which are not necessarily in phase with the cropping seasons (Huijsmans et al., 2018).

We concluded our model-inventory comparison by computing the correlation of monthly NH_3 emission rates in each model grid cell (see **Figure 2(d)**, **(f)**, and **(h)**). CLM5 can capture a large portion of emission hotspots of CMIP6 over the US, Europe, India, China, and South America. With MASAGE, our estimate shows good agreement over mid-range emission regions, in North America, South America, Europe, and Southern Africa. CLM5 differs the most from EDGAR among the three inventories. The resemblance with CMIP6 and MASAGE

indicates that our NH₃ scheme has allowed CLM5 to produce reasonable NH_3 emission inputs for CAM4-chem simulations over most high to medium emission hotspots. It is also noteworthy that the magnitude and spatial distribution of NH_3 emission among inventories are also not consistent. Since environmental conditions control the rate of biological and chemical processes that release NH_3, processes such as urea hydrolysis and NH_4^+/NH_3 equilibrium can induce further inventory uncertainties (Hoesly et al., 2018). Inter-inventory uncertainties are also attributable to the choice of global and/or regional emission factors, which is crucial to reflect different agricultural procedures across the world, such as fertilization methods and fertilizer types, but not always well represented in global inventories (Paulot and Jacob, 2014; Riddick et al., 2016; Zhang et al., 2018).
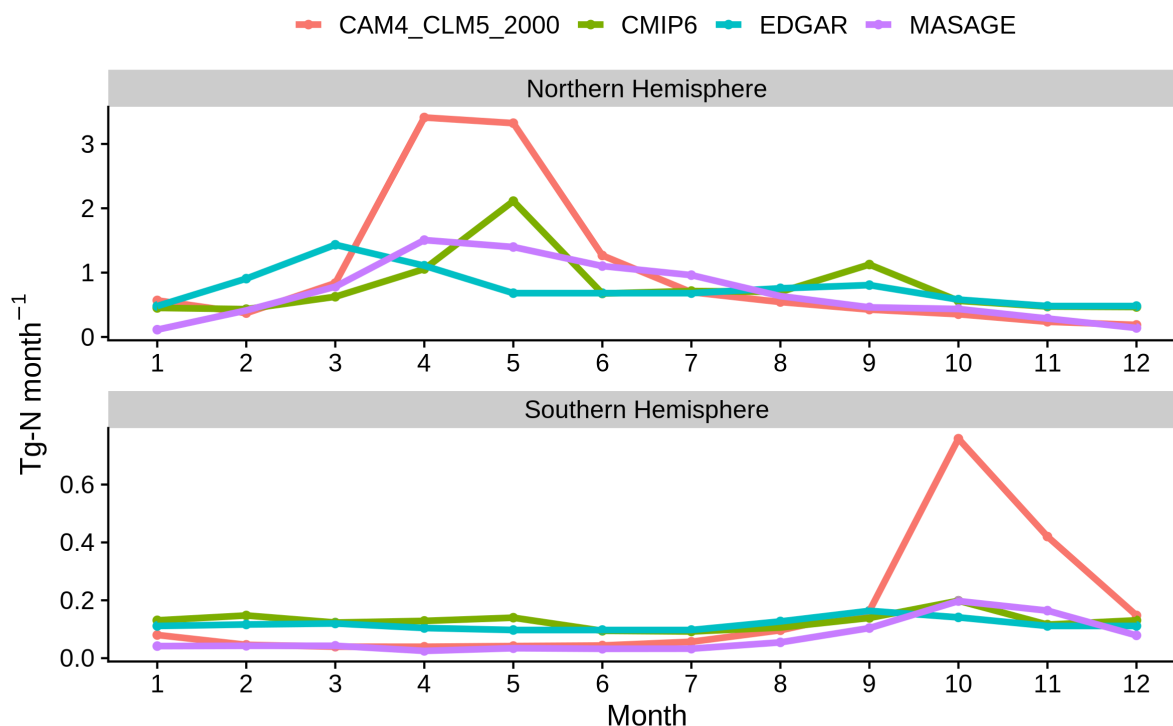
Figure 3. Monthly NH_3 emission associated with synthetic fertilizer use in the Northern and South Hemisphere estimated by CLM5, CMIP6, EDGAR, and MASAGE.

3.2 Atmospheric NH₃ concentration

535 Previous studies have evaluated the reactive nitrogen processes in CESM against satellite and ground observations, e.g., depositional fluxes of NH_3 and NH_4^+ (Lamarque et al., 2013), and ground concentration of gaseous NH_3 (He et al., 2015). Here, we estimated the CAM4-chem simulated annual-mean atmospheric NH_3 using two different sets of fertilizer-induced emissions: 1) simulated by our revised CLM5 ([CAM4_CLM5_2000]), and; 2) one prescribed

540 from CMIP6 ([CAM4_CMIP6_2000]). Source of non-fertilizer related NH_3 and other reactive gases were identical in these two cases. **Figure 4** shows these results, aggregated to column total NH_3, alongside the 8-year annual-average IASI satellite retrievals.

Both simulations can capture the high NH_3 zones observed by IASI over the US, South America, and Europe, with global and regional R values > 0.5, indicating a good correlation

545 between the modeled results and observations. However, both [CAM4_CLM5_2000] and [CAM4_CMIP6_2000] NH_3 are generally lower than IASI. One except is over India, in which [CAM4_CLM5_2000] estimates higher than IASI with a regional β of 3.3. [CAM4_CLM5_2000] matches IASI better over the US (regional $\beta = 0.9$), where CLM5 estimates high emission rates. Even more significant underestimation is seen in

550 [CAM4_CMIP6_2000] (regional $\beta = 0.5$) over the US. The magnitudes of NMB and MFB of [CAM4_CLM5_2000] are less negative than [CAM4_CMIP6_2000] in most regions, reflecting that using CLM5 as NH_3 emission input reduces the model NH_3 underestimation of CAM4-chem with the default CMIP6 inventory.

Mild differences are seen in North America and northeastern China, which are both

555 intense agricultural regions; the discrepancies are likely attributable to the mismatch in crop growth map between CLM5 and the real world. Larger differences are shown over India and Western Europe, indicating the low-biases in the model of emission from tropical biomass burning regions (Whitburn et al., 2017; Van Damme et al., 2018).

We further compared the NH_3 burden of a run with online NH_3 emission but prescribed

560 N deposition, i.e., [CAM4_CLM5_CLIM_2000], against IASI to examine whether enabling the online bidirectional exchange can improve the estimation of NH_3 in CLM5. The global-total NH_3 emission increases by 0.45% by enabling dynamic nitrogen deposition raised ([CAM4_CLM5_2000]–[CAM4_CLM5_CLIM_2000]) while the regional changes are not

uniform (**Figure S3)**. The most prominent increase is found in Asia (+0.06 Tg-N yr^{-1} or +0.9%

565 regionally), while the largest decrease is seen in Europe (–0.03 Tg-N yr^{-1} or –2.9%). When

compared with IASI, [CAM4_CLM5_2000] and [CAM4_CLM5_CLIM_2000] both have

closer-to-one β and closer-to-zero NMB and MFB than [CAM4_CMIP6_2000] (**Figure S4)**,

indicating that coupling the land-atmosphere N-cycle could reduce model low-bias.
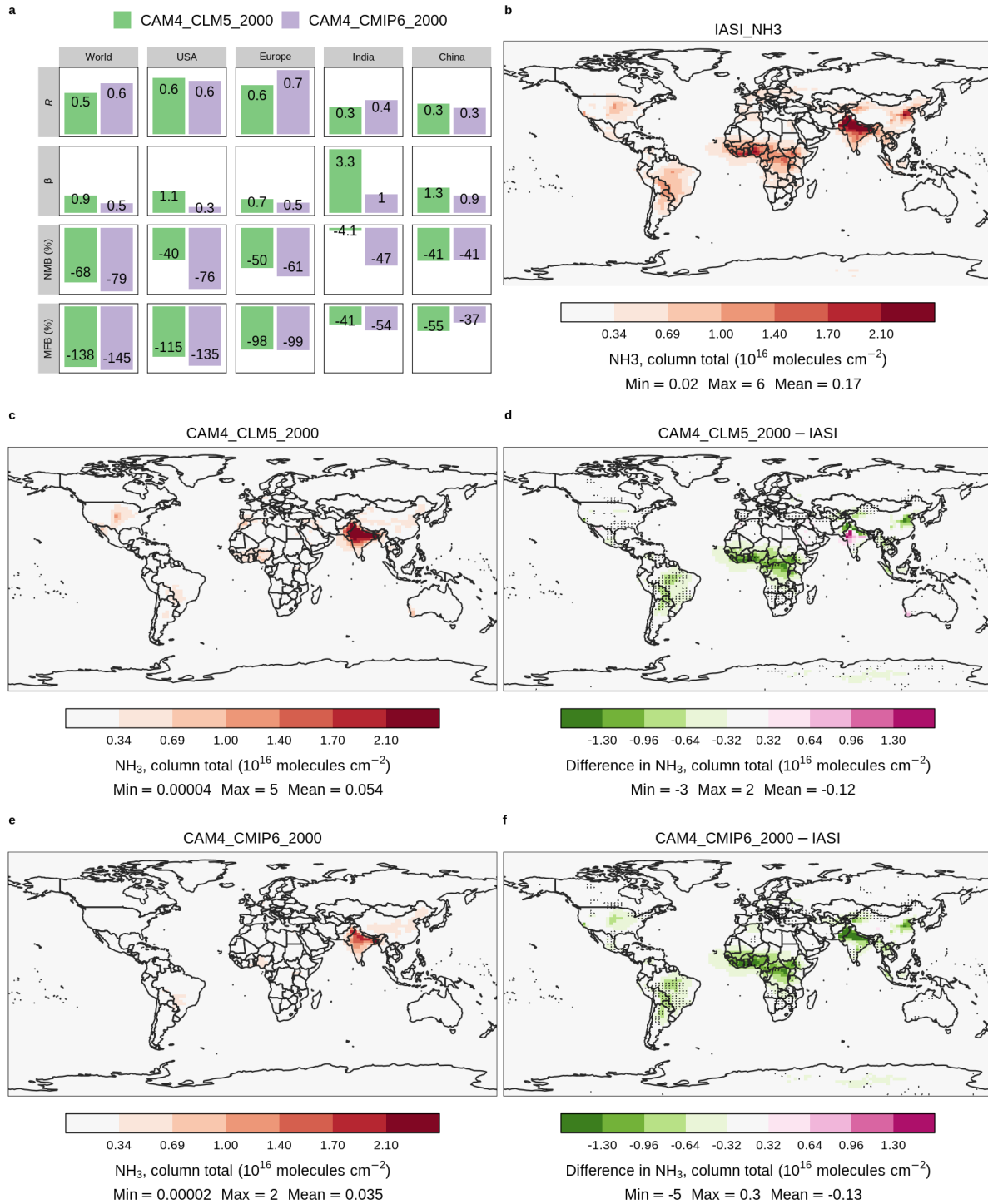
Figure 4. Annual-mean atmospheric NH₃ estimated by CAM4-chem with online CLM5 simulation and CMIP6 emission inventory as inputs of fertilizer-induced NH₃ emission, which are aliased as [CAM4_CLM5_2000] and [CAM4_CMIP6_2000], respectively. Panel **(a)** summarizes the correlation analysis between the two simulations and the IASI satellite retrievals. Panels **(b)**, **(c)**, and **(e)** show the column NH₃ concentration of IASI and the two cases correspondingly. Panels **(d)**, and **(f)** show concentration differences between each case and the IASI observations. Overlaying black dots in the difference maps indicate grid-cells with a high statistically significant

spatiotemporal correlation (i.e., $R^2 > 50\%$, $p < 0.05$) between CLM5 and IASI. Color scales are saturated at respective values, and ranges of values are shown in the legend titles.

580 **3.3 When 30% more synthetic fertilizer is applied globally – a case study to reveal the importance of nitrogen deposition and aerosol-climate effect on NH$_3$ emission and grain production in a future scenario**

Fertilizer use is predicted to increase by >30% of 2000-level to boost grain production to meet the fast-growing food demand by 2050 (FAO, 2007). Such injection of soil nitrogen will not **585** only enhance soil NH$_3$ emission, but also alter atmospheric NH$_4^+$ formation and its subsequent climate effects and deposition, which will induce secondary impacts on crop growth and NH$_3$ re-emission. Here, we used the modified CLM5 and CAM4-chem to attribute such secondary impacts to nitrogen deposition and aerosol-climate effect. We performed this case study by scaling up the amounts of synthetic fertilizer application by 30% globally as input to the **590** simulations detailed in **Table 1**. The application rate of manure fertilizer was assumed to be at the same level in both scenarios since increased usage would likely raise nitrogen leakage during production and transportation that are difficult to quantify and beyond the scope of this study.

Table 4 summarizes the changes in annual-total fertilizer-induced NH$_3$ emission **595** estimated by these simulations when the global synthetic fertilizer use rises to 130% of the 2000 level. The total fertilization rate at the 2050 level was 117 Tg-N yr^{-1} (or +21% from the present-day total fertilization rate at 96.5 Tg-N yr^{-1}, which is comparable to ~100 Tg-N yr^{-1} suggested by FAO (2008)). We also computed the nitrogen leakage ratio (NLR) and nitrogen use efficiency (NUE) for each case. NLR maintains at ~15% for [CAM4_CLM5_2000] and **600** [CAM4_CLM5_2050] while NUE decreases from 23% to 22%, respectively, indicating that the crops are under nitrogen surplus under this future fertilization scenario. This is also confirmed by the reduced ratio of crop uptake to fertilization from ~130% to ~115% (**Table S3**).

Table 4. Summary of N fluxes in the simulations averaged over 20 years.

	Fertilization (Tg-N yr^{-1})	NH$_3$ Emission (Tg-N yr^{-1})	NLR* (%)	Grain N Harvested (Tg-N yr^{-1})	NUE[#] (%)
CAM4_CLM5_2000	96.5	14.2	14.7	21.9	22.7
CAM4_CLM5_2050	117.0	17.5	14.9	25.5	21.8
CAM4_CLM5_CLIM_2050	117.0	17.0	14.5	24.3	20.8
CAM4_CLM5_NDEP_2050	117.0	17.9	15.3	25.6	21.9

* Nitrogen Leakage Ratio (NLR) = NH$_3$ Emission / Fertilization
[#] Nitrogen Use Efficiency (NUE) = Grain N Harvested / Fertilization

605

Figure 5(b) shows the changes of the fully coupled case, [CAM4_CLM5_2050], which estimated that global emission will rise by 3.3 Tg-N yr^{-1} more of fertilizer-associated NH$_3$ emission than the baseline case, i.e., [CAM4_CLM5_2000]. The super-linear increase in NH$_3$ emission (+24%) relative to total fertilizer (+21%) is associated with sub-linear rise in nitrification (+17%), crop uptake (+5.8%) and other loss processes of soil NH$_4^+$. It is a result of a larger tendency of NH$_3$ volatilization compared to other loss processes during the 20 days of intensive fertilizer application period, highlighting that our model modifications enabled CLM5 to simulate the dynamic competing processes of soil nitrogen. Regionally, changes in Indian and Chinese emissions are the highest, generally overlapping with the high fertilization zones (**Figure S5**), totaling a +1.6 Tg-N yr^{-1} or +24% for Asia relative to the baseline.

610

615
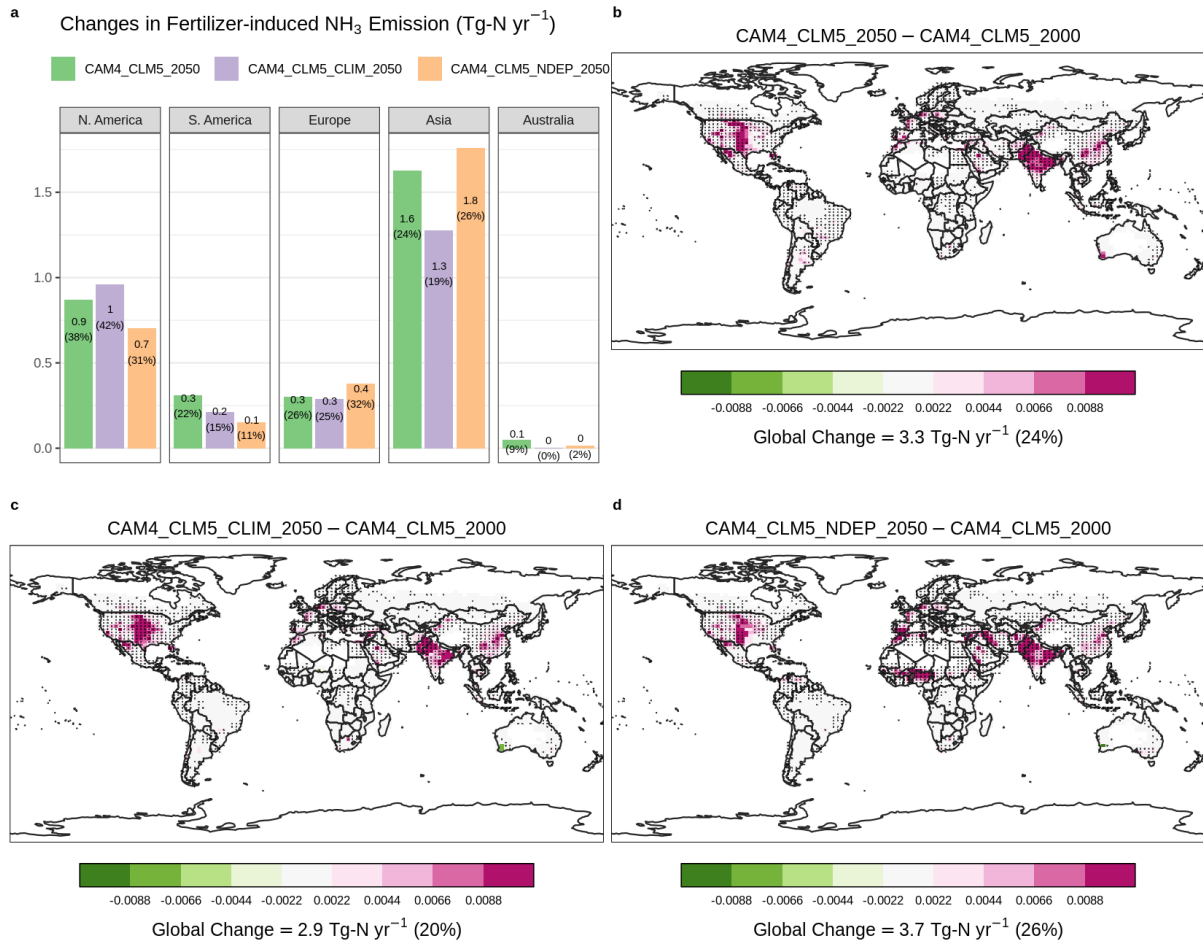
Figure 5. Changes in annual-total fertilizer-induced NH₃ emission at the present-day synthetic fertilizer usage to the future scenario. Panel **(a)** summarizes regional changes relative to [CAM4_CLM5_2000]. Spatial distribution of the changes from [CAM4_CLM5_2000] with [CAM4_CLM5_2050] is shown in panel **(b)**, with [CAM4_CLM5_CLIM_2050] in **(c)**, and with [CAM4_CLM5_NDEP_2050] in **(d)**. Overlaying black dots indicate grid-cells with a statistically significant difference under two-sample t-tests (i.e., $p < 0.05$) between corresponding simulations. Color scales are saturated at respective values.

CLM5 assumes a harvest efficiency of 85% (Lawrence et al., 2018). [CAM4_CLM5_2050] estimated that, with nitrogen deposition and aerosol climate effect, 243 Tg yr⁻¹ (in dry matter, hereinafter) more grain is produced than the baseline (see **Figure 6(b)**). Such enhancement is found dominantly over the food-producing regions over Europe (+76 Tg yr⁻¹ or +17%) and North America (+78 Tg yr⁻¹ or +17%). The grain production in Asia has divergent responses to induced fertilizers (increases in northern China and decreases in southern India). This results in a smaller Asian grain production increase of +55 Tg yr⁻¹ (+4%).
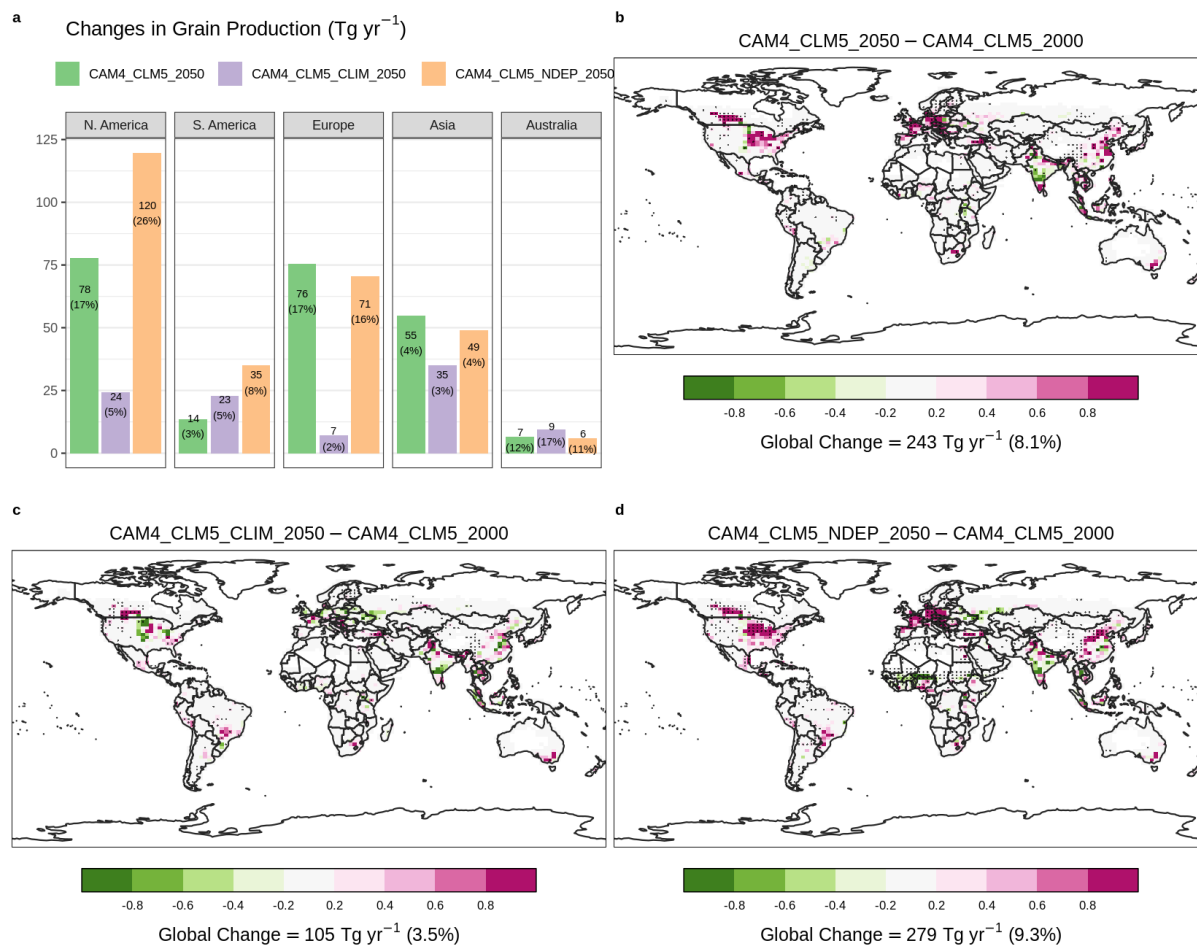
Figure 6. Same as **Figure 5** but for annual-total grain production (in Tg-(dry matter) yr^{-1}).

635

We evaluated the impacts of dynamic processes in our simulations by comparing the fully-coupled simulation with other cases, i.e., the effects of including dynamic nitrogen deposition (Δ_{ndep} = [CAM4_CLM5_2050]–[CAM4_CLM5_CLIM_2050]) and aerosol-climate interaction (Δ_{clim} = [CAM4_CLM5_2050]–[CAM4_CLM5_NDEP_2050]) in the model.

640

As agricultural NH$_3$ is injected to the atmosphere, it rapidly neutralizes other acidic chemicals and facilitates the formation of particulate NH$_4^+$. Some of the nitrogen particles return to the surface via deposition, sequentially fuel soil NH$_3$ emission and boost crop growth. Our simulation shows that nitrogen deposition is enhanced by 1.6 Tg-N yr^{-1}, mostly in the US and India (**Figure S8(a)**). It translates to an increased NH$_3$ emission by 0.47 Tg-N yr^{-1} globally

645 (**Figure 7**), but the enhancement is seen mostly in India. On the contrary, there is a decrease in NH_3 emission over the US. The increase/decrease is associated with a higher/lower annual-mean surface temperature (**Figure S9(a)**). In addition to directly enhancing the tendency of NH_3 volatilization, a warmer surface temperature also shortens crop growth and grain filling period, resulting in lower crop nitrogen uptake (**Figure S10(a)**) and less grain production

650 (**Figure 8(a)**), e.g., in India. Though the impacts of the larger nitrogen deposition in Δ_{ndep} are not evenly distributed spatially, it boosts grain production by 138 Tg-N globally.

On the other hand, we expected the sulfate aerosols induced by agricultural NH_3, which directly increases aerosol albedo, would reduce the amount of insolation reaching the Earth's surface. Comparing the 2000- and 2050-fertilization levels, our fully coupled simulation

655 estimated a –0.005 W m^{-2} in global downward radiative flux (i.e., cooling), which is virtually negligible compared to the 16-model mean total anthropogenic aerosol radiative forcing of –0.27 W m^{-2} reported in Myhre et al. (2013). Though the global impact is also negligible (+0.004 W m^{-2}), Δ_{clim} reveals a substantial regional cooling at the surface level (**Figure S11(b)**) largely because there are more prognostic dusts in [CAM4_CLM5_2050] over Sub-Saharan Africa

660 than prescribed in [CAM4_CLM5_NDEP_2050]. Such cooling effect results in lower surface temperature (**Figure S9(b)**) and also suppressing the formation of particulate sulfate (**Figure S12(b)**). These changes in surface temperature reduce NH_3 emission substantially over Africa, while promoting NH_3 volatilization in India and the North and South America, resulting in a net decrease by 0.41 Tg-N yr^{-1} globally. Grain production decreases by 36 Tg-N yr^{-1} in Δ_{clim},

665 indicating that the warming induced by aerosol-radiation interaction partly offsets the benefit of nitrogen deposition as an extra input of soil NH_4^+ for crop growth and yield, though the deposition rate is increased slightly over the US (**Figure S8(b)**).
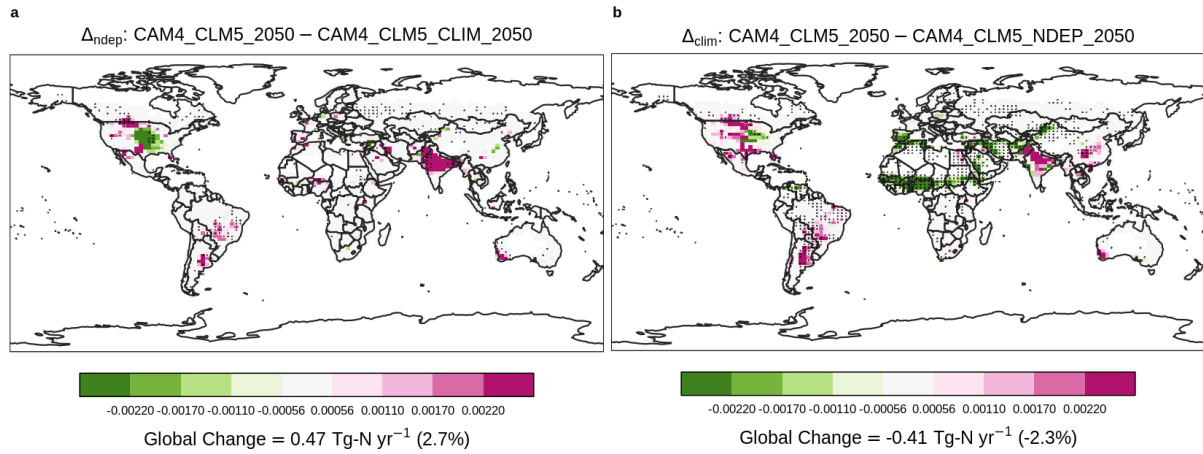
Figure 7. Contrasting the difference in NH$_3$ emission (Tg-N yr^{-1}). Overlaying black dots indicate grid-cells with a statistically significant difference under two-sample t-tests (i.e., $p < 0.05$) between corresponding simulations. Only results of grid-cells with croplands are shown.
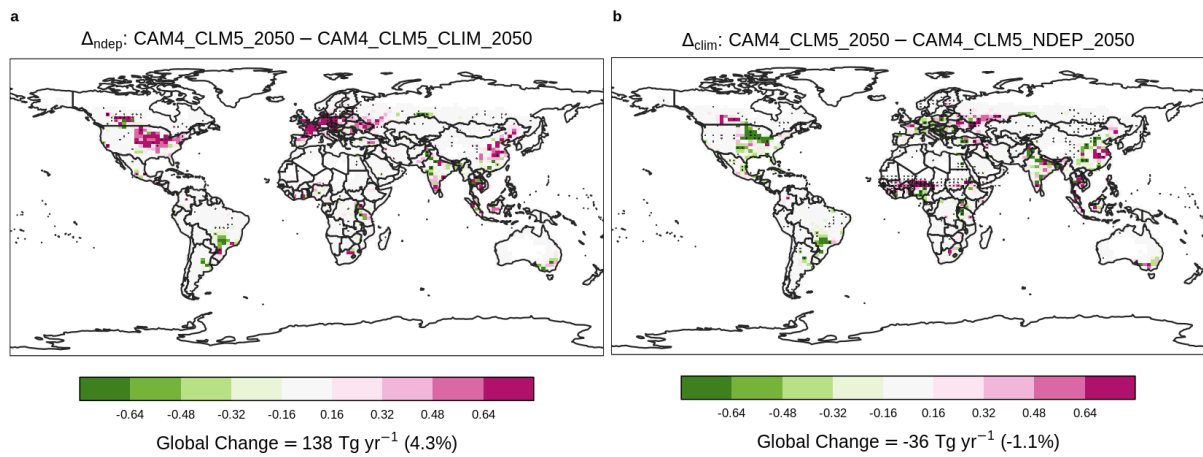
Figure 8. Contrasting the difference in grain production (Tg-dry-matter yr^{-1}). Overlaying black dots indicate grid-cells with a statistically significant difference under two-sample t-tests (i.e., $p < 0.05$) between corresponding simulations. Only results of grid-cells with croplands are shown.

4. Conclusions

In this study, we implemented into the land and biogeochemical model, CLM5, new mechanistic schemes to better represent fertilizer-induced NH_3 emission from agricultural soil. Our modifications allowed CLM5 and CAM4-chem to dynamically exchange fluxes associated with reactive nitrogen deposition and NH_3 emission. These new features enabled CESM2 to perform a more reliable estimation of soil NH_3 emission and atmospheric NH_3 concentration than using constant emission inventory values under dynamic climate and environmental conditions. We verified that a fully coupled simulation case, [CAM4_CLM5_2000], produced an estimation of NH_3 emission that agrees fairly well spatially and temporally with the emission inventories, MASAGE (Paulot et al., 2014) and CMIP6 (Hoesly et al., 2018), especially over high-emission regions (see **Figure 2**). When compared to the IASI satellite observations (Van Damme et al., 2018), online NH_3 emission input in CLM5 reduces the low-biases exhibited in CAM4-chem estimation of atmospheric NH_3 using the CMIP6 NH_3 emission inventory.

Our modifications also enabled us to understand how NH_3 emission influences aerosol formation and aerosol radiative effect, and their secondary impacts on the re-emission of NH_3 and grain production. Our fully coupled simulation, [CAM4_CLM5_2000], re-creates the spatial distribution of the emission hotspots observed by satellite over intensive agricultural regions including China, India, Europe, and the US (see **Figure 4**). We also estimate that if the synthetic fertilizer use was to increase by 30% from 2000's level, NH_3 emission would rise by 3.3 Tg-N yr^{-1} globally (see **Figure 5**). We further performed two simulations to highlight the importance of including a fully coupled nitrogen cycle in the model. Our results showed that lacking dynamic N deposition would underestimate NH_3 emission and grain production under intensified fertilization while ignoring the aerosol-radiation interaction would lead to overestimation.

This study demonstrates a modeling approach to estimate the climatic and environmental sensitivity of NH_3 emission, with a focus on sources associated with manure and synthetic fertilizer only. Other primary sources of atmospheric NH_3 include manure management and application (47%), ocean (16%), and biomass burning (11%) (e.g., Bouwman et al., 1997; Sutton et al., 2013; Paulot et al., 2014, 2015). Unlike soil emission whereby the volatilization of NH_3 depends on a series of biogeochemical processes, emissions associated with manure management are typically estimated differently, e.g., collecting activity data and

emission factors from factory managers, and installing monitoring instruments at outlets of confined facilities, e.g., animal factories (Bouwman et al., 1997; Paulot et al., 2014). Manure production, storage, and usage can be collected by surveying practices adopted by farmers while its associated NH_3 emission can be estimated using source-specific emission factors and weather data, especially dominant factors such as air temperature, wind speed, and humidity. Fire emission directly injects the reactive nitrogen into the atmosphere, and satellite measurement is capable of capturing such short-term ammonia blooms (Van Damme et al., 2017). We did not include manure management in our study due to the high uncertainty and data insufficiency for validation. It is noteworthy that manure is attributable up to ~60 % of total soil NH_3 emission (Vira et al., 2020) and hence shall warrant further research efforts in terms of its downstream impact on ecosystems via nitrogen deposition and aerosol radiative effect.

We also incorporated a prognostic parameterization for canopy capture of the emitted NH_3, which is an improvement when compared to previous studies that assigned blanket reduction factors to all vegetated land types (Bouwman et al., 1997; Riddick et al., 2016; Vira et al., 2020). Despite such addition, our model still shows systematic high-biases, implying room for improvement, including further calibration of the canopy capture effects against field measurements. Another source of uncertainties stems from the model's initial soil NH_4^+ content, which determines the potential emission rate of NH_3. The overestimation by CLM5 in this study may point to the more-fertile-than-reality soil conditions in the model, highlighting the need for a more realistic soil nitrogen map compiled by field surveys to better constrain the initial conditions for the model. We also note that such field surveys, especially in underrepresented regions with low data coverage, would also be useful to infer a soil pH map that constraints the uncertainty in simulations using a constant pH, like those reported in this study.

Our schemes simplified the fate of NH_3 captured by the canopy and assumed that such NH_3 is returned to the soil and becomes immediately accessible to plants, soil microbes, and bacteria, due to limited knowledge of the consequences of the canopy capturing process. A chamber study suggested that soybean can absorb up to 20 kg-N ha^{-1} of NH_3 via leaf capturing (Hutchinson et al., 1972), which is a significant amount compared to average fertilizer use for soybean of 13–45 kg-N ha^{-1} in CLM5. On the other hand, concentrated NH_3 could damage leaf

740   tissues if the contacting plant fails to metabolize or detoxify such a reactive gas in time (Nemitz et al., 2001). The remaining captured NH_3 on the leaf surface can return to the soil via throughfall, but its magnitude is difficult to measure. These unspecified processes may induce uncertainties in our simulations, especially for plant growth and soil NH_4^+ content. This knowledge gap points to a demand for more field experiments to investigate the impacts of

745   these processes.

        FAO projects that fertilizer use will be increased by >30% (FAO, 2007) to boost food production to meet the fast-growing food demand by 2050. Such additional fertilizer injects mineral nitrogen into the soil that further fuels the volatilization of NH_3 spontaneously and hence promotes the subsequent formation of aerosol particles. This study shows the nonlinear

750   impacts of nitrogen deposition and aerosol radiative effect on the environment. Thus, our work makes it possible to evaluate the intertwined consequences of such soaring use of fertilizer on NH_3 emission, atmospheric aerosols composition, and the corresponding aerosol-climate effect. Our results can provide scientific information to aid stakeholders in evaluating various global and regional plans for mitigating climate change and safeguarding a sustainable environment.

755

Code availability

The modified codes of CESM2 developed in this study will be available will be available upon request.

760

Author Contribution

All co-authors participated in designing the experiments. KMF and MVM developed the model code. KMF performed the simulations. KMF prepared the manuscript with contributions from all co-authors.

765

Competing Interests

The authors declare that they have no conflict of interest.

Acknowledgments

770   This work was supported by the Research Grants Council (RGC) General Research Fund (Project #: 14323116) and the National Natural Science Foundation of China (NSFC)/Research Grants Council (RGC) (Grant no.: N_CUHK440/20) awarded by the Research Grants Council (RGC) of the University Grants Committee of Hong Kong to A. P. K. Tai. M. Val Martin acknowledges funding from the Leverhulme Trust through a Leverhulme Research Centre
775   Award (RC-2015-029) and the UKRI Future Leaders Fellowship Programme (MR/T019867/1). We would also like to acknowledge the high-performance computing support from Cheyenne (doi:10.5065/D6RX99HX) provided by NCAR's Computational and Information Systems Laboratory, sponsored by the National Science Foundation. We also think the reviewers of this manuscript for their constructive feedback.

780

References

Ansari, A. S. and Pandis, S. N.: Response of inorganic PM to precursor concentrations, 32, 2706–2714, https://doi.org/10.1021/es971130j, 1998.

Balasubramanian, S., Koloutsou-Vakakis, S., McFarland, D. M., and Rood, M. J.: Reconsidering emissions of ammonia from chemical fertilizer usage in midwest USA, 120, 6232–6246, https://doi.org/10.1002/2015JD023219, 2015.

Balasubramanian, S., Nelson, A., Koloutsou-Vakakis, S., Lin, J., Rood, M. J., Myles, L. T., and Bernacchi, C.: Evaluation of DeNitrification DeComposition model for estimating ammonia fluxes from chemical fertilizer application, 237–238, 123–134, https://doi.org/10.1016/j.agrformet.2017.02.006, 2017.

Beeckman, F., Motte, H., and Beeckman, T.: Nitrification in agricultural soils: impact, actors and mitigation, 50, 166–173, https://doi.org/10.1016/j.copbio.2018.01.014, 2018.

Behera, S. N. and Sharma, M.: Transformation of atmospheric ammonia and acid gases into components of PM2.5: An environmental chamber study, 19, 1187–1197, https://doi.org/10.1007/s11356-011-0635-9, 2012.

Bodirsky, B. L., Popp, A., Lotze-Campen, H., Dietrich, J. P., Rolinski, S., Weindl, I., Schmitz, C., Müller, C., Bonsch, M., Humpenöder, F., Biewald, A., and Stevanovic, M.: Reactive nitrogen requirements to feed the world in 2050 and potential to mitigate nitrogen pollution, 5, https://doi.org/10.1038/ncomms4858, 2014.

Bonan, G. B., Levis, S., Kergoat, L., and Oleson, K. W.: Landscapes as patches of plant functional types: An integrating concept for climate and ecosystem models, 16, 5-1-5–23, https://doi.org/10.1029/2000gb001360, 2002.

Bouwman, A. F., Lee, D. S., Asman, W. A. H., Dentener, F. J., Van Der Hoek, K. W., and Olivier, J. G. J.: A global high-resolution emission inventory for ammonia, 11, 561–587, https://doi.org/10.1029/97GB02266, 1997.

Bouwman, A. F., Boumans, L. J. M., and Batjes, N. H.: Estimation of global NH$_3$ volatilization loss from synthetic fertilizers and animal manure applied to arable lands and grasslands: AMMONIA EMISSION FROM FERTILIZERS, Global Biogeochem. Cycles, 16, 8-1-8–14, https://doi.org/10.1029/2000GB001389, 2002.

Clarisse, L., Clerbaux, C., Dentener, F., Hurtmans, D., and Coheur, P. F.: Global ammonia distribution derived from infrared satellite observations, 2, 479–483, https://doi.org/10.1038/ngeo551, 2009.

Clarisse, L., Shephard, M. W., Dentener, F., Hurtmans, D., Cady-Pereira, K., Karagulian, F., Van Damme, M., Clerbaux, C., and Coheur, P. F.: Satellite monitoring of ammonia: A case study of the San Joaquin Valley, 115, 1–15, https://doi.org/10.1029/2009JD013291, 2010.

Crippa, M., Guizzardi, D., Muntean, M., Schaaf, E., Dentener, F., Van Aardenne, J. A., Monni, S., Doering, U., Olivier, J. G. J., Pagliari, V., and Janssens-Maenhout, G.: Gridded emissions

of air pollutants for the period 1970-2012 within EDGAR v4.3.2, 10, 1987–2013, https://doi.org/10.5194/essd-10-1987-2018, 2018.

820   Van Damme, M., Clarisse, L., Heald, C. L., Hurtmans, D., Ngadi, Y., Clerbaux, C., Dolman, A. J., Erisman, J. W., and Coheur, P. F.: Global distributions, time series and error characterization of atmospheric ammonia (NH3) from IASI satellite observations, 14, 2905–2922, https://doi.org/10.5194/acp-14-2905-2014, 2014.

Van Damme, M., Whitburn, S., Clarisse, L., Clerbaux, C., Hurtmans, D., and Coheur, P. F.:
825   Version 2 of the IASI NH3 neural network retrieval algorithm: Near-real-time and reanalysed datasets, 10, 4905–4914, https://doi.org/10.5194/amt-10-4905-2017, 2017.

Van Damme, M., Clarisse, L., Whitburn, S., Hadji-Lazaro, J., Hurtmans, D., Clerbaux, C., and Coheur, P. F.: Industrial and agricultural ammonia point sources exposed, 564, 99–103, https://doi.org/10.1038/s41586-018-0747-1, 2018.

830   Drewniak, B., Song, J., Prell, J., Kotamarthi, V. R., and Jacob, R.: Modeling agriculture in the Community Land Model, 6, 495–515, https://doi.org/10.5194/gmd-6-495-2013, 2013.

Dutta, B., Congreves, K. A., Smith, W. N., Grant, B. B., Rochette, P., Chantigny, M. H., and Desjardins, R. L.: Improving DNDC model to estimate ammonia loss from urea fertilizer application in temperate agroecosystems, 106, 275–292, https://doi.org/10.1007/s10705-016-
835   9804-z, 2016.

Emmons, L. K., Walters, S., Hess, P. G., Lamarque, J. F., Pfister, G. G., Fillmore, D., Granier, C., Guenther, A., Kinnison, D., Laepple, T., Orlando, J., Tie, X., Tyndall, G., Wiedinmyer, C., Baughcum, S. L., and Kloster, S.: Description and evaluation of the Model for Ozone and Related chemical Tracers, version 4 (MOZART-4), 3, 43–67, https://doi.org/10.5194/gmd-3-
840   43-2010, 2010.

European Environment Agency: Ammonia (NH3) emissions, 2010.

European Environment Agency: EMEP/EEA air pollutant emission inventory guidebook 2013: Exhaust emissions from road transport, 160, https://doi.org/10.2800/92722, 2013.

Fangmeier, A., Hadwiger-Fangmeier, A., Van der Eerden, L., and Jäger, H.-J.: Effects of
845   atmospheric ammonia on vegetation—A review, Environmental Pollution, 86, 43–82, https://doi.org/10.1016/0269-7491(94)90008-6, 1994.

FAO: Re-estimation of Global Fertilizer Requirement for 2015, 2030 and 2050, 2007.

Food and Agriculture Organization of the United Nations: Current world fertilizer trends and outlook to 2011/12, 2008.

850   Gardner, W. R.: Movement of Nitrogen in Soil, in: Soil Nitrogen, John Wiley & Sons, Ltd, 550–572, https://doi.org/10.2134/agronmonogr10.c15, 1965.

Gilhespy, S. L., Anthony, S., Cardenas, L., Chadwick, D., del Prado, A., Li, C., Misselbrook, T., Rees, R. M., Salas, W., Sanz-Cobena, A., Smith, P., Tilston, E. L., Topp, C. F. E., Vetter,

S., and Yeluripati, J. B.: First 20 years of DNDC (DeNitrification DeComposition): Model evolution, 292, 51–62, https://doi.org/10.1016/j.ecolmodel.2014.09.004, 2014.

Gu, B. B. B., Ge, Y., Ren, Y., Xu, B., Luo, W., Jiang, H., Gu, B. B. B., and Chang, J.: Atmospheric Reactive Nitrogen in China: Sources, Recent Trends, and Damage Costs, 46, 9420–9427, https://doi.org/10.1021/es301446g, 2012.

Guenther, A. B., Jiang, X., Heald, C. L., Sakulyanontvittaya, T., Duhl, T., Emmons, L. K., and Wang, X.: The model of emissions of gases and aerosols from nature version 2.1 (MEGAN2.1): An extended and updated framework for modeling biogenic emissions, 5, 1471–1492, https://doi.org/10.5194/gmd-5-1471-2012, 2012.

Guthrie, S., Dunkerley, F., Tabaqchali, H., Harshfield, A., Ioppolo, B., and Manville, C.: Impact of ammonia emissions from agriculture on biodiversity: An evidence synthesis, https://doi.org/10.7249/rr2695, 2018.

He, J., Zhang, Y., Glotfelty, T., He, R., Bennartz, R., Rausch, J., and Sartelet, K.: Decadal simulation and comprehensive evaluation of CESM/CAM5.1 with advanced chemistry, aerosol microphysics, and aerosol-cloud interactions, J. Adv. Model. Earth Syst., 7, 110–141, https://doi.org/10.1002/2014MS000360, 2015.

Hoesly, R. M., Smith, S. J., Feng, L., Klimont, Z., Janssens-Maenhout, G., Pitkanen, T., Seibert, J. J., Vu, L., Andres, R. J., Bolt, R. M., Bond, T. C., Dawidowski, L., Kholod, N., Kurokawa, J., Li, M., Liu, L., Lu, Z., Moura, M. C. P., O'Rourke, P. R., and Zhang, Q.: Historical (1750–2014) anthropogenic emissions of reactive gases and aerosols from the Community Emissions Data System (CEDS), 11, 369–408, https://doi.org/10.5194/gmd-11-369-2018, 2018.

Van Hove, L. W. A., Koops, A. J., Adema, E. H., Vredenberg, W. J., and Pieters, G. A.: Analysis of the uptake of atmospheric ammonia by leaves of Phaseolus vulgaris L., 21, 1759–1763, https://doi.org/10.1016/0004-6981(87)90115-6, 1987.

Huang, X., Song, Y., Li, M., Li, J., Huo, Q., Cai, X., Zhu, T., Hu, M., and Zhang, H.: A high-resolution ammonia emission inventory in China, 26, 1–14, https://doi.org/10.1029/2011GB004161, 2012.

Huijsmans, J. F. M., Vermeulen, G. D., Hol, J. M. G., and Goedhart, P. W.: A model for estimating seasonal trends of ammonia emission from cattle manure applied to grassland in the Netherlands, 173, 231–238, https://doi.org/10.1016/j.atmosenv.2017.10.050, 2018.

Hurrell, J. W., Hack, J. J., Shea, D., Caron, J. M., and Rosinski, J.: A new sea surface temperature and sea ice boundary dataset for the community atmosphere model, 21, 5145–5153, https://doi.org/10.1175/2008JCLI2292.1, 2008.

Hurrell, J. W., Holland, M. M., Gent, P. R., Ghan, S., Kay, J. E., Kushner, P. J., Lamarque, J.-F., Large, W. G., Lawrence, D., Lindsay, K., Lipscomb, W. H., Long, M. C., Mahowald, N., Marsh, D. R., Neale, R. B., Rasch, P., Vavrus, S., Vertenstein, M., Bader, D., Collins, W. D., Hack, J. J., Kiehl, J., and Marshall, S.: The Community Earth System Model: A Framework

for Collaborative Research, 130204122247009, https://doi.org/10.1175/bams-d-12-00121, 2013.

Hurtt, G. C., Chini, L. P., Frolking, S., Betts, R. A., Feddema, J., Fischer, G., Fisk, J. P.,
895 Hibbard, K., Houghton, R. A., Janetos, A., Jones, C. D., Kindermann, G., Kinoshita, T., Klein Goldewijk, K., Riahi, K., Shevliakova, E., Smith, S., Stehfest, E., Thomson, A., Thornton, P., van Vuuren, D. P., and Wang, Y. P.: Harmonization of land-use scenarios for the period 1500-2100: 600 years of global gridded annual land-use transitions, wood harvest, and resulting secondary lands, 109, 117–161, https://doi.org/10.1007/s10584-011-0153-2, 2011.

900 Hutchinson, G. L., Millington, R. J., and Peters, D. B.: Atmospheric Ammonia: Absorption by Plant Leaves, 175, 771–772, https://doi.org/10.1126/science.175.4023.771, 1972.

Ianniello, A., Spataro, F., Esposito, G., Allegrini, I., Hu, M., and Zhu, T.: Chemical characteristics of inorganic ammonium salts in PM2.5 in the atmosphere of Beijing (China), 11, 10803–10822, https://doi.org/10.5194/acp-11-10803-2011, 2011.

905 Institute for the Study of Earth, Oceans, and Space, University of New Hampshire: DNDC v9.5 Scientific Basis and Processes, 2017.

Janssens-Maenhout, G., Crippa, M., Guizzardi, D., Dentener, F., Muntean, M., Pouliot, G., Keating, T., Zhang, Q., Kurokawa, J., Wankmüller, R., Denier van der Gon, H., Kuenen, J. J. P., Klimont, Z., Frost, G., Darras, S., Koffi, B., and Li, M.: HTAP_v2.2: a mosaic of regional
910 and global emission grid maps for 2008 and 2010 to study hemispheric transport of air pollution, Atmos. Chem. Phys., 15, 11411–11432, https://doi.org/10.5194/acp-15-11411-2015, 2015.

Krupa, S. V.: Effects of atmospheric ammonia (NH3) on terrestrial vegetation: a review, Environmental Pollution, 124, 179–221, https://doi.org/10.1016/S0269-7491(02)00434-7, 2003.

915 Lamarque, J. F., Dentener, F., McConnell, J., Ro, C. U., Shaw, M., Vet, R., Bergmann, D., Cameron-Smith, P., Dalsoren, S., Doherty, R., Faluvegi, G., Ghan, S. J., Josse, B., Lee, Y. H., Mackenzie, I. A., Plummer, D., Shindell, D. T., Skeie, R. B., Stevenson, D. S., Strode, S., Zeng, G., Curran, M., Dahl-Jensen, D., Das, S., Fritzsche, D., and Nolan, M.: Multi-model mean nitrogen and sulfur deposition from the atmospheric chemistry and climate model
920 intercomparison project (ACCMIP): Evaluation of historical and projected future changes, 13, 7997–8018, https://doi.org/10.5194/acp-13-7997-2013, 2013.

Lamarque, J.-F., Emmons, L. K., Hess, P. G., Kinnison, D. E., Tilmes, S., Vitt, F., Heald, C. L., Holland, E. A., Lauritzen, P. H., Neu, J., Orlando, J. J., Rasch, P. J., and Tyndall, G. K.: CAM-chem: description and evaluation of interactive atmospheric chemistry in the
925 Community Earth System Model, Geosci. Model Dev., 5, 369–411, https://doi.org/10.5194/gmd-5-369-2012, 2012.

Lawrence, D., Fisher, R., Koven, C., Swenson, S., and Vertenstein, M.: Technical Description of version 5.0 of the Community Land Model (CLM), http://www.cesm.ucar.edu/models/cesm2/land/CLM50_Tech_Note.pdf, February 2018.

930   Lawrence, D. M., Fisher, R. A., Koven, C. D., Oleson, K. W., Swenson, S. C., Bonan, G., Collier, N., Ghimire, B., Kampenhout, L., Kennedy, D., Kluzek, E., Lawrence, P. J., Li, F., Li, H., Lombardozzi, D., Riley, W. J., Sacks, W. J., Shi, M., Vertenstein, M., Wieder, W. R., Xu, C., Ali, A. A., Badger, A. M., Bisht, G., Broeke, M., Brunke, M. A., Burns, S. P., Buzan, J., Clark, M., Craig, A., Dahlin, K., Drewniak, B., Fisher, J. B., Flanner, M., Fox, A. M., Gentine,
935   P., Hoffman, F., Keppel-Aleks, G., Knox, R., Kumar, S., Lenaerts, J., Leung, L. R., Lipscomb, W. H., Lu, Y., Pandey, A., Pelletier, J. D., Perket, J., Randerson, J. T., Ricciuto, D. M., Sanderson, B. M., Slater, A., Subin, Z. M., Tang, J., Thomas, R. Q., Val Martin, M., and Zeng, X.: The Community Land Model Version 5: Description of New Features, Benchmarking, and Impact of Forcing Uncertainty, J. Adv. Model. Earth Syst., 11, 4245–4287,
940   https://doi.org/10.1029/2018MS001583, 2019.

Lawrence, P. J. and Chase, T. N.: Representing a new MODIS consistent land surface in the Community Land Model (CLM 3.0), 112, https://doi.org/10.1029/2006JG000168, 2007.

Levis, S., Badger, A., Drewniak, B., Nevison, C., and Ren, X.: CLMcrop yields and water requirements: avoided impacts by choosing RCP 4.5 over 8.5, 146, 501–515,
945   https://doi.org/10.1007/s10584-016-1654-9, 2018.

Li, C., Frolking, S., and Frolking, T. A.: A model of nitrous oxide evolution from soil driven by rainfall events: 1. Model structure and sensitivity, 97, 9759–9776, https://doi.org/10.1029/92JD00509, 1992.

Li, C., Salas, W., Zhang, R., Krauter, C., Rotz, A., and Mitloehner, F.: Manure-DNDC: A
950   biogeochemical process model for quantifying greenhouse gas and ammonia emissions from livestock manure systems, 93, 163–200, https://doi.org/10.1007/s10705-012-9507-z, 2012.

Lin, B. Le, Sakoda, A., Shibasaki, R., and Suzuki, M.: A modelling approach to global nitrate leaching caused by anthropogenic fertilisation, Water Research, 1961–1968 pp., https://doi.org/10.1016/S0043-1354(00)00484-X, 2001.

955   Liu, X., Tai, A. P. K., and Fung, K. M.: Responses of surface ozone to future agricultural ammonia emissions and subsequent nitrogen deposition through terrestrial ecosystem changes, 21, 17743–17758, https://doi.org/10.5194/acp-21-17743-2021, 2021.

Lombardozzi, D. L., Lu, Y., Lawrence, P. J., Lawrence, D. M., Swenson, S., Oleson, K. W., Wieder, W. R., and Ainsworth, E. A.: Simulating Agriculture in the Community Land Model
960   Version 5, J. Geophys. Res. Biogeosci., 125, https://doi.org/10.1029/2019JG005529, 2020.

Lu, X. K., Mo, J. M., and Dong, S. F.: Effects of nitrogen deposition on forest biodiversity: A review, Shengtai Xuebao/ Acta Ecologica Sinica, 5532–5548 pp., https://doi.org/10.1016/S1872-2032(09)60012-3, 2008.

van Marle, M. J. E., Kloster, S., Magi, B. I., Marlon, J. R., Daniau, A.-L., Field, R. D., Arneth,
965   A., Forrest, M., Hantson, S., Kehrwald, N. M., Knorr, W., Lasslop, G., Li, F., Mangeon, S., Yue, C., Kaiser, J. W., and van der Werf, G. R.: Biomass Burning emissions for CMIP6 (v1.2), https://doi.org/10.22033/ESGF/input4MIPs.1117, 2016.

van Marle, M. J. E., Kloster, S., Magi, B. I., Marlon, J. R., Daniau, A.-L., Field, R. D., Arneth, A., Forrest, M., Hantson, S., Kehrwald, N. M., Knorr, W., Lasslop, G., Li, F., Mangeon, S., Yue, C., Kaiser, J. W., and van der Werf, G. R.: Historic global biomass burning emissions for CMIP6 (BB4CMIP) based on merging satellite observations with proxies and fire models (1750–2015), Geosci. Model Dev., 10, 3329–3357, https://doi.org/10.5194/gmd-10-3329-2017, 2017.

Meinshausen, M., Vogel, E., Nauels, A., Lorbacher, K., Meinshausen, N., Etheridge, D. M., Fraser, P. J., Montzka, S. A., Rayner, P. J., Trudinger, C. M., Krummel, P. B., Beyerle, U., Canadell, J. G., Daniel, J. S., Enting, I. G., Law, R. M., Lunder, C. R., O'Doherty, S., Prinn, R. G., Reimann, S., Rubino, M., Velders, G. J. M., Vollmer, M. K., Wang, R. H. J., and Weiss, R.: Historical greenhouse gas concentrations for climate modelling (CMIP6), Geosci. Model Dev., 10, 2057–2116, https://doi.org/10.5194/gmd-10-2057-2017, 2017.

Metzger, S.: Gas/aerosol partitioning: 1. A computationally efficient model, J. Geophys. Res., 107, 4312, https://doi.org/10.1029/2001JD001102, 2002.

Myhre, G., Samset, B. H., Schulz, M., Balkanski, Y., Bauer, S., Berntsen, T. K., Bian, H., Bellouin, N., Chin, M., Diehl, T., Easter, R. C., Feichter, J., Ghan, S. J., Hauglustaine, D., Iversen, T., Kinne, S., Kirkevåg, A., Lamarque, J.-F., Lin, G., Liu, X., Lund, M. T., Luo, G., Ma, X., van Noije, T., Penner, J. E., Rasch, P. J., Ruiz, A., Seland, Ø., Skeie, R. B., Stier, P., Takemura, T., Tsigaridis, K., Wang, P., Wang, Z., Xu, L., Yu, H., Yu, F., Yoon, J.-H., Zhang, K., Zhang, H., and Zhou, C.: Radiative forcing of the direct aerosol effect from AeroCom Phase II simulations, Atmos. Chem. Phys., 13, 1853–1877, https://doi.org/10.5194/acp-13-1853-2013, 2013.

National Oceanic and Atmospheric Administration: Atmospheric Ammonia: Sources and Fate - A Review of Ongoing Federal Research and Future Need, Journal of Molecular Liquids, 2000.

Neale, R. B., Richter, J. H., Conley, A. J., Park, S., Lauritzen, P. H., Gettelman, A., Williamson, D. L., Rasch, P. J., Vavrus, S. J., Taylor, M. A., Collins, W. D., Zhang, M., and Lin, S.-J.: Description of the NCAR Community Atmosphere Model (CAM 4.0), 224, 2010.

Nemitz, E., Milford, C., and Sutton, M. A.: A two-layer canopy compensation point model for describing bi-directional biosphere-atmosphere exchange of ammonia, 127, 815–833, https://doi.org/10.1256/smsqj.57305, 2001.

Neu, J. L. and Prather, M. J.: Toward a more physical representation of precipitation scavenging in global chemistry models: Cloud overlap and ice physics and their impact on tropospheric ozone, 12, 3289–3310, https://doi.org/10.5194/acp-12-3289-2012, 2012.

Nevison, C., Hess, P., Riddick, S., and Ward, D.: Denitrification, leaching, and river nitrogen export in the Community Earth System Model, 8, 272–291, https://doi.org/10.1002/2015MS000573, 2016.

Paulot, F. and Jacob, D. J.: Hidden Cost of U.S. Agricultural Exports: Particulate Matter from Ammonia Emissions, 48, 903–908, https://doi.org/10.1021/es4034793, 2014.

Paulot, F., Jacob, D. J., Pinder, R. W., Bash, J. O., Travis, K., and Henze, D. K.: Ammonia emissions in the United States, European Union, and China derived by high-resolution inversion of ammonium wet deposition data: Interpretation with a new agricultural emissions inventory (MASAGE_NH3), 119, 4343–4364, https://doi.org/10.1002/2013JD021130, 2014.

1010 Paulot, F., Jacob, D. J., Johnson, M. T., Bell, T. G., Baker, A. R., Keene, W. C., Lima, I. D., Doney, S. C., and Stock, C. A.: Global oceanic emission of ammonia: Constraints from seawater and atmospheric observations, 29, 1165–1178, https://doi.org/10.1002/2015GB005106, 2015.

Pleim, J. E., Bash, E. O., Walker, J. T., and Cooter, E. J.: Development and evaluation of an 1015 ammonia bidirectional flux parameterization for air quality models, 118, 3794–3806, https://doi.org/10.1002/jgrd.502622013, 2013.

Pleim, J. E., Ran, L., Appel, W., Shephard, M. W., and Cady-Pereira, K.: New Bidirectional Ammonia Flux Model in an Air Quality Model Coupled With an Agricultural Model, J. Adv. Model. Earth Syst., 11, 2934–2957, https://doi.org/10.1029/2019MS001728, 2019.

1020 Portmann, F. T., Siebert, S., and Döll, P.: MIRCA2000-Global monthly irrigated and rainfed crop areas around the year 2000: A new high-resolution data set for agricultural and hydrological modeling, 24, n/a-n/a, https://doi.org/10.1029/2008gb003435, 2010.

Riddick, S., Ward, D., Hess, P., Mahowald, N., Massad, R., and Holland, E.: Estimate of changes in agricultural terrestrial nitrogen pathways and ammonia emissions from 1850 to 1025 present in the Community Earth System Model, 13, 3397–3426, https://doi.org/10.5194/bg-13-3397-2016, 2016.

Saikawa, E., Schlosser, C. A., and Prinn, R. G.: Global modeling of soil nitrous oxide emissions from natural processes, 27, 972–989, https://doi.org/10.1002/gbc.20087, 2013.

Saikawa, E., Prinn, R. G., Dlugokencky, E., Ishijima, K., Dutton, G. S., Hall, B. D., 1030 Langenfelds, R., Tohjima, Y., Machida, T., Manizza, M., Rigby, M., O'Doherty, S., Patra, P. K., Harth, C. M., Weiss, R. F., Krummel, P. B., Van Der Schoot, M., Fraser, P. J., Steele, L. P., Aoki, S., Nakazawa, T., and Elkins, J. W.: Global and regional emissions estimates for N2O, 14, 4617–4641, https://doi.org/10.5194/acp-14-4617-2014, 2014.

Shou, W., Zong, H., Ding, P., and Hou, L.: A modelling approach to assess the effects of 1035 atmospheric nitrogen deposition on the marine ecosystem in the Bohai Sea, China, 208, 36–48, https://doi.org/10.1016/j.ecss.2018.04.025, 2018.

Snider, G., Weagle, C. L., Murdymootoo, K. K., Ring, A., Ritchie, Y., Stone, E., Walsh, A., Akoshile, C., Anh, N. X., Balasubramanian, R., Brook, J., Qonitan, F. D., Dong, J., Griffith, D., He, K., Holben, B. N., Kahn, R., Lagrosas, N., Lestari, P., Ma, Z., Misra, A., Norford, L. 1040 K., Quel, E. J., Salam, A., Schichtel, B., Segev, L., Tripathi, S., Wang, C., Yu, C., Zhang, Q., Zhang, Y., Brauer, M., Cohen, A., Gibson, M. D., Liu, Y., Martins, J. V., Rudich, Y., and Martin, R. V.: Variation in global chemical composition of PM 2.5 : emerging results from SPARTAN, 16, 9629–9653, https://doi.org/10.5194/acp-16-9629-2016, 2016.

Sutton, M. A.: The surface/atmosphere exchange of ammonia, University of Edinburgh, 1990.

1045   Sutton, M. A., Pitcairn, C. E., and Fowler, D.: The exchange of ammonia between the atmosphere and plant communities, 24, 301–393, 1993.

Sutton, M. A., Reis, S., Riddick, S. N., Dragosits, U., Nemitz, E., Theobald, M. R., Tang, Y. S., Braban, C. F., Vieno, M., Dore, A. J., Mitchell, R. F., Wanless, S., Daunt, F., Fowler, D., Blackall, T. D., Milford, C., Flechard, C. R., Loubet, B., Massad, R., Cellier, P., Personne, E.,
1050   Coheur, P. F., Clarisse, L., Van Damme, M., Ngadi, Y., Clerbaux, C., Skjøth, C. A., Geels, C., Hertel, O., Kruit, R. J. W., Pinder, R. W., Bash, J. O., Walker, J. T., Simpson, D., Horváth, L., Misselbrook, T. H., Bleeker, A., Dentener, F., and de Vries, W.: Towards a climate-dependent paradigm of ammonia emission and deposition, 368, https://doi.org/10.1098/rstb.2013.0166, 2013.

1055   Tian, D. and Niu, S.: A global analysis of soil acidification caused by nitrogen addition, 10, https://doi.org/10.1088/1748-9326/10/2/024019, 2015.

Tie, X. and Cao, J.: Aerosol pollution in China: Present and future impact on environment, 7, 426–431, https://doi.org/10.1016/j.partic.2009.09.003, 2009.

US Environmental Protection Agency: National Emission Inventory (NEI) Report, 2014.

1060   Vira, J., Hess, P., Melkonian, J., and Wieder, W. R.: An improved mechanistic model for ammonia volatilization in Earth system models: Flow of Agricultural Nitrogen version 2 (FANv2), Geosci. Model Dev., 13, 4459–4490, https://doi.org/10.5194/gmd-13-4459-2020, 2020.

Vira, J., Hess, P., Ossohou, M., and Galy-Lacaux, C.: Evaluation of interactive and prescribed
1065   agricultural ammonia emissions for simulating atmospheric composition in CAM-Chem, Biosphere Interactions/Atmospheric Modelling/Troposphere/Chemistry (chemical composition and reactions), https://doi.org/10.5194/acp-2021-538, 2021.

Wang, J., Xing, J., Mathur, R., Pleim, J. E., Wang, S., Hogrefe, C., Gan, C. M., Wong, D. C., and Hao, J.: Historical trends in PM2.5-related premature mortality during 1990–2010 across
1070   the Northern Hemisphere, 125, 400–408, https://doi.org/10.1289/EHP298, 2017.

Wesely, M. L.: Parameterization of Surface Resistances to Gaseous Dry Deposition in Regional-Scale Numerical Models, 23, 1293–1304, https://doi.org/10.1016/j.atmosenv.2007.10.058, 1989.

Whitburn, S., Van Damme, M., Clarisse, L., Hurtmans, D., Clerbaux, C., and Coheur, P. F.:
1075   IASI-derived NH3 enhancement ratios relative to CO for the tropical biomass burning regions, 17, 12239–12252, https://doi.org/10.5194/acp-17-12239-2017, 2017.

Willem Asman; Mark A. Sutton: Ammonia : emission , atmospheric transport and deposition, 27–48, 1998.

Wortman, E., Tomaszewski, T., Waldner, P., Schleppi, P., Thimonier, A., Eugster, W.,
1080   Buchmann, N., and Sievering, H.: Atmospheric nitrogen deposition and canopy retention influences on photosynthetic performance at two high nitrogen deposition Swiss forests, 64, 17216, https://doi.org/10.3402/tellusb.v64i0.17216, 2012.

Xing, Y. F., Xu, Y. H., Shi, M. H., and Lian, Y. X.: The impact of PM2.5 on the human respiratory system, https://doi.org/10.3978/j.issn.2072-1439.2016.01.19, 2016.

1085   Yang, Y., Ruan, Z., Wang, X., Yang, Y., Mason, T. G., Lin, H., and Tian, L.: Short-term and long-term exposures to fine particulate matter constituents and health: A systematic review and meta-analysis, 247, 874–882, https://doi.org/10.1016/j.envpol.2018.12.060, 2019.

Zhang, J. and Liu, M. G.: Observations on nutrient elements and sulphate in atmospheric wet depositions over the northwest Pacific coastal oceans - Yellow Sea, 47, 173–189,
1090   https://doi.org/10.1016/0304-4203(94)90107-4, 1994.

Zhang, L., Chen, Y., Zhao, Y., Henze, D. K., Zhu, L., Song, Y., Paulot, F., Liu, X., Pan, Y., Lin, Y., and Huang, B.: Agricultural ammonia emissions in China: Reconciling bottom-up and top-down estimates, 18, 339–355, https://doi.org/10.5194/acp-18-339-2018, 2018.

Zhang, Y. and Niu, H.: The development of the DNDC plant growth sub-model and the
1095   application   of   DNDC   in   agriculture: A   review,   230,   271–282, https://doi.org/10.1016/j.agee.2016.06.017, 2016.

Zhao, Y., Zhang, L., Tai, A. P. K., Chen, Y., and Pan, Y.: Responses of surface ozone air quality to anthropogenic nitrogen deposition in the Northern Hemisphere, 17, 9781–9796, https://doi.org/10.5194/acp-17-9781-2017, 2017.

1100   Zheng, Y., Xue, T., Zhang, Q., Geng, G., Tong, D., Li, X., and He, K.: Air quality improvements and health benefits from China's clean air action since 2013, 12, https://doi.org/10.1088/1748-9326/aa8a32, 2017.

Zhu, L., Henze, D., Bash, J., Jeong, G.-R., Cady-Pereira, K., Shephard, M., Luo, M., Paulot, F., and Capps, S.: Global evaluation of ammonia bidirectional exchange and livestock diurnal
1105   variation schemes, Atmos. Chem. Phys., 15, 12823–12843, https://doi.org/10.5194/acp-15-12823-2015, 2015.